8342 *Inorg. Chem.* **2009**, *48*, 8342–8356
DOI: 10.1021/ic900975y

Inorganic Chemistry
Article

Molecular Oxygen and Sulfur Reactivity of a Cyclotriveratrylene Derived Trinuclear Copper(I) Complex

Debabrata Maiti,[†] Julia S. Woertink,[‡] Reza A. Ghiladi,[†] Edward I. Solomon,[‡] and Kenneth D. Karlin*,[†]

[†]*Department of Chemistry, The Johns Hopkins University, Baltimore, Maryland 21218, and* [‡]*Department of Chemistry, Stanford University, Stanford, California 94305*

Received May 18, 2009

Our continuing efforts into developing copper coordination chemistry relevant to dioxygen-processing copper proteins has led us to design and synthesize a cyclotriveratrylene (CTV)-based trinucleating ligand, CTV-TMPA, which employs tetradentate tris(2-pyridylmethyl)-amine chelates (TMPA) for their copper ion binding sites. Binding of three copper ions per CTV-TMPA unit was established by various chemical and spectroscopic methods such as UV−vis and resonance Raman (rR) spectroscopies. The following complexes were observed: A tricopper(I) complex $[(\text{CTV-TMPA})\text{Cu}^{\text{I}}_3]^{3+}$ (**1**), a CO adduct $[(\text{CTV-TMPA})\text{Cu}^{\text{I}}_3(\text{CO})_3]^{3+}$ (**1-CO**; $\nu(\text{C}{=}\text{O}) = 2094\ \text{cm}^{-1}$), a triphenylphosphine adduct $[(\text{CTV-TMPA})\text{Cu}^{\text{I}}_3(\text{PPh}_3)_3]^{3+}$ (**1-PPh$_3$**), a tricopper(II) complex $[(\text{CTV-TMPA})\text{Cu}^{\text{II}}_3]^{3+}$ (**1-Ox**), and its tris-monochloride or tris-monobromide adducts. Also, introduction of dioxygen to the −80 °C solutions of **1** leads to O_2-adducts, the first example of a synthetic copper complex which can stabilize a mononuclear Cu^{II}-superoxo and dinuclear peroxo species simultaneously within one complex {[Cu] = 1.53 mM in THF: (μ-1,2-peroxo complex, λ_{max} = 543 (ε 9650) nm): $\nu(\text{O}-\text{O}) = 825$ ($(\Delta^{18}\text{O}_2) = -47$) cm^{-1}; $\nu(\text{Cu}-\text{O}) = 506$ ($(\Delta^{18}\text{O}_2) = -26$) cm^{-1}: (superoxo complex, λ_{max} = 427 (ε 3150) nm): $\nu(\text{O}-\text{O}) = 1129$ ($(\Delta^{18}\text{O}_2) = -60$) cm^{-1}; $\nu(\text{Cu}-\text{O}) = 463$ ($(\Delta^{18}\text{O}_2) = -27$) cm^{-1}}. Elemental sulfur reacts reversibly with **1** leading to a (proposed) hexanuclear species $[\{(\text{CTV-TMPA})\text{Cu}^{\text{II}}_3\}_2(\mu\text{-}1,2\text{-}S_2^{2-})_3]^{6+}$ (**1-S**) {λ_{max} = 544 (ε 7270) nm }, possessing one dicopper(II)-disulfide structural type: {THF solvent} $\nu(\text{S}-\text{S}) = 489$ ($(\Delta^{34}\text{S}) = -10$) cm^{-1}; $\nu(\text{Cu}-\text{S}) = 307$ ($(\Delta^{34}\text{S}) = -5$) cm^{-1}}. Derivation of spectroscopic, structural, and chemical conclusions were aided by the study of a close mononuclear analogue with one pyridyl group of the TMPA parent possessing a 6-CH_2OCH_3 substituent, this being part of the CTV-TMPA architecture.

Introduction

Biological systems containing multinuclear copper centers have motivated synthetic inorganic chemists to attempt to mimic biosite structure, spectroscopy, and active-site function.[1−7] As this topic pertains to copper ion, binuclear copper centers occur in the O_2-carrier hemocyanins and the related tyrosinase monooxygenases, and synthetic model systems for such proteins are now abundant.[5,6,8,9] Copper clusters are well established for the "multicopper oxidases" (MCOs).[10−15] These extensively studied proteins reveal synergism between two or more copper sites in the activation of dioxygen.[10,11,16] The currently well-characterized members include ascorbate oxidase (AO) (Figure 1, top), laccase (Lc), ceruloplasmin (Cp), Fet3, bilurubin oxidase (BO), and CueO, In these proteins, the electron-transfer cycle is conveniently mediated by four copper sites which store oxidizing power upon complete four-electron reduction of dioxygen to water prior to delivering oxidizing equivalents in a sequential manner to a substrate such as

*To whom correspondence should be addressed. E-mail: karlin@jhu.edu.

(1) Solomon, E.; Sarangi, R.; Woertink, J.; Augustine, A.; Yoon, J.; Ghosh, S. *Acc. Chem. Res.* **2007**, *40*, 581–591.
(2) Biomimetic Inorganic Chemistry. Holm, R. H., Solomon, E. I., Eds.; In *Chem. Rev.* **2004**; Vol. *104* (2).
(3) Fenton, D. E.; Okawa, H. *J. Chem. Soc., Dalton Trans.* **1993**, 1349–1357.
(4) Karlin, K. D. *Science* **1993**, *261*, 701–708.
(5) Mirica, L. M.; Ottenwaelder, X.; Stack, T. D. P. *Chem. Rev.* **2004**, *104*, 1013–1045.
(6) Lewis, E. A.; Tolman, W. B. *Chem. Rev.* **2004**, *104*, 1047–1076.
(7) Lee, Y.; Karlin, K. D. Highlights of Copper Protein Active-Site Structure/Reactivity and Synthetic Model Studies. In *Concepts and Models in Bioinorganic Chemistry*; Metzler-Nolte, N. , Kraatz, H.-B., Eds.; Wiley-VCH: New York, 2006; pp 363−395.
(8) Op't Holt, B. T.; Vance, M. A.; Mirica, L. M.; Heppner, D. E.; Stack, T. D. P.; Solomon, E. I. *J. Am. Chem. Soc.* **2009**, *131*, 6421–6438.
(9) Hatcher, L. Q.; Karlin, K. D. *J. Biol. Inorg. Chem.* **2004**, *9*, 669–683.
(10) Yoon, J.; Fujii, S.; Solomon, E. I. *Proc. Nat. Acad. Sci.* **2009**, *106*, 6585–6590.
(11) Solomon, E. I.; Augustine, A. J.; Yoon, J. *Dalton Trans.* **2008**, 3921–3932.
(12) Solomon, E. I.; Chen, P.; Metz, M.; Lee, S.-K.; Palmer, A. E. *Angew. Chem., Int. Ed.* **2001**, *40*, 4570–4590.
(13) Messerschmidt, A. *Adv. Inorg. Chem.* **1993**, *40*, 121–185.
(14) Lee, D.-H.; Lucchese, B.; Karlin, K. D. Multimetal Oxidases. In *Bio-coordination chemistry*; Que, L., Jr., Tolman, W. B., Eds.; Elsevier Ltd: Oxford, 2004; Vol. *8*, pp 437−457.
(15) Bento, I.; Carrondo, M.; Lindley, P. *J. Biol. Inorg. Chem.* **2006**, *11*, 539–547.
(16) Kataoka, K.; Sugiyama, R.; Hirota, S.; Inoue, M.; Urata, K.; Minagawa, Y.; Seo, D.; Sakurai, T. *J. Biol. Chem.* **2009**, *284*, 14405–14413.

 Published on Web 08/10/2009

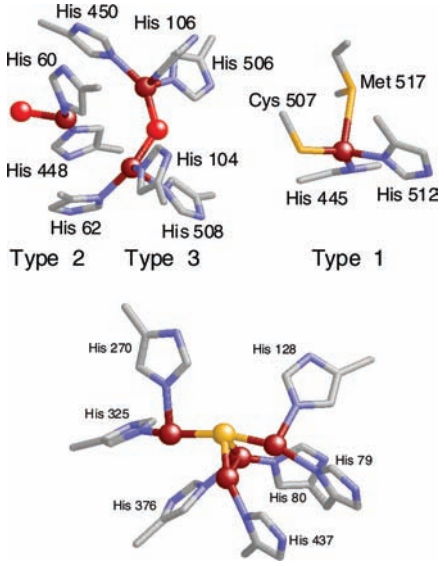

Figure 1. Top: Active site structure of ascorbate oxidase showing the type 2/type 3 catalytic triad, and the type 1 "blue" copper electron-transfer center. Coordinates (1AOZ) were taken from the Protein Data Bank (Brookhaven) and displayed using the program Rasmol. Bottom: Active site structure of Cu_Z sites in N_2OR. Coordinates (1QN1) were taken from the Protein Data Bank (Brookhaven) and displayed using the program Rasmol.

ascorbate or iron(II) ion. X-ray crystallographic determinations of the most prominent member of this series, AO, along with others, confirm that three of these four copper ions are intimately engaged to form a catalytic triad, one type 2 (mononuclear) and one type 3 (couple binuclear) copper center. The fourth copper ion is a distinct type-1 (or "blue") copper center that oxidizes substrates which bind nearby and most likely contributes to the overall stoichiometry by long-range (~12.5 Å in AO) but through-bond electron-transfer to the trinuclear cluster.

A multicopper cluster also exists in the active site of nitrous oxide reductase (N_2OR) (Figure 1, bottom) which possesses four copper ions in close proximity to form a (histidine)$_7$Cu$_4$(μ_4-S) cluster (referred to as Cu_Z).[1,17,18] This mediates the final step in bacterial denitrification, $N_2O + 2e^- + 2H^+ \rightarrow H_2O + N_2$ and plays a critical environmental role by preventing release of greenhouse gas nitrous oxide. On the basis of biochemical and spectroscopic studies, particulate methane monooxygenase (pMMO) (found in methanotrophic eubacteria) and ammonia monooxygenase (AMO) (ammonia-oxidizing eubacteria) are believed by some to contain copper cluster.[19,20] These oxygenases catalyze a number of industrially important transformations, including the conversion of methane to methanol, ethane hydroxylation, and the oxidation of other hydrocarbons, halogenated organics, and carbon monoxide.

A variety of trinuclear copper model compounds have been obtained by self-assembly reactions.[21−34] In an alternative approach, conformationally constrained trinucleating ligands have been introduced to bind three metal ions in close proximity. Most of these are rather flexible and fail to impose a perfectly well-defined arrangement of the metals. Some of the synthetic ligand systems employed from the groups of Karlin,[35−38] Kim,[39] Itoh,[40,41] Tolman,[42] Casella,[43] Fenton,[3,44] and Chan[45]are depicted in Chart 1. Our earlier efforts[35−38] into modeling the active sites of copper-cluster containing enzymes led us to synthesize trinucleating ligands including mesitylene-based organics (Chart 1, MesPy1, MesPy2)[46] which employ tridentate copper-chelates as their copper binding sites. Structural characterization of the resulting tricopper complexes revealed that the trimethyl-mesitylene motif may not provide the cluster-like geometry required for Cu^I_3/O_2 intramolecular reactivity, since the complexes have two copper centers located on one side of the mesityl plane, with the third on the other "opposite" side. In a similar context, Kim and Itoh employed 1,3,5-triethyl-benzene "steering" motifs showing that this forces all

(17) Haltia, T.; Brown, K.; Tegoni, M.; Cambillau, C.; Saraste, M.; Mattila, K.; Djinovic-Carugo, K. *Biochem. J.* **2003**, *369*, 77–88.
(18) Ghosh, S.; Gorelsky, S. I.; DeBeerGeorge, S.; Chan, J. M.; Cabrito, I.; Dooley, D. M.; Moura, J. J. G.; Moura, I.; Solomon, E. I. *J. Am. Chem. Soc.* **2007**, *129*, 3955–3965.
(19) Chan, S. I.; Yu, S. S.-F. *Acc. Chem. Res.* **2008**, *41*, 969–979.
(20) Himes, R. A.; Karlin, K. D. *Curr. Opin. Chem. Biol.* **2009**, *13*, 119–131.
(21) Szeverényl, Z.; Knopp, U.; Zuberbühler, A. D. *Helv. Chim. Acta* **1982**, *65*, 2529–2539.
(22) Hubberstey, P.; Russell, C. E. *J. Chem. Soc., Chem. Commun.* **1995**, 959–960.
(23) Chaudhuri, P.; Karpenstein, I.; Winter, M.; Butzlaff, C.; Bill, E.; Trautwein, A. X.; Flörke, U.; Haupt, H.-J. *J. Chem. Soc., Chem. Commun.* **1992**, 321–322.
(24) Root, D. E.; Henson, M. J.; Machonkin, T.; Mukherjee, P.; Stack, T. D. P.; Solomon, E. I. *J. Am. Chem. Soc.* **1998**, *120*, 4982–4990.
(25) Bonnefous, C.; Bellec, N.; Thummel, R. P. *Chem. Commun.* **1999**, 1243–1244.
(26) Kodera, M.; Tachi, Y.; Kita, T.; Kobushi, H.; Sumi, Y.; Kano, K.; Shiro, M.; Koikawa, M.; Tokii, T.; Ohba, M.; Okawa, H. *Inorg. Chem.* **2000**, *39*, 226–234.
(27) Liu, X. M.; de Miranda, M. P.; McInnes, E. J. L.; Kilner, C. A.; Halcrow, M. A. *Dalton Trans.* **2004**, 59–64.
(28) Mirica, L. M.; Stack, T. D. P. *Inorg. Chem.* **2005**, *44*, 2131–2133.
(29) Chen, J.; Wang, X.; Shao, Y.; Zhu, J.; Zhu, Y.; Li, Y.; Xu, Q.; Guo, Z. *Inorg. Chem.* **2007**, *46*, 3306–3312.
(30) DiNicola, C.; Karabach, Y. Y.; Kirillov, A. M.; Monari, M.; Pandolfo, L.; Pettinari, C.; Pombeiro, A. J. L. *Inorg. Chem.* **2007**, *46*, 221–230.
(31) Manzur, J.; Mora, H.; Vega, A.; Spodine, E.; Venegas-Yazigi, D.; Garland, M. T.; ElFallah, M. S.; Escuer, A. *Inorg. Chem.* **2007**, *46*, 6924–6932.
(32) Song, Y. F.; vanAlbada, G. A.; Tang, J.; Mutikainen, I.; Turpeinen, U.; Massera, C.; Roubeau, O.; Costa, J. S.; Gamez, P.; Reedijk, J. *Inorg. Chem.* **2007**, *46*, 4944–4950.
(33) Groysman, S.; Holm, R. H. *Inorg. Chem.* **2009**, *48*, 621–627.
(34) Di Nicola, C.; Garau, F.; Karabach, Y. Yu.; Martins, L. M. D. R. S.; Monari, M.; Pandolfo, L.; Pettinari, C.; Pombeiro, A. J. L. *Eur. J. Inorg. Chem.* **2009**, 666–676.
(35) Karlin, K. D.; Gan, Q.-F.; Farooq, A.; Liu, S.; Zubieta, J. *Inorg. Chim. Acta* **1989**, *165*, 37–39.
(36) Karlin, K. D.; Gan, Q.-F.; Farooq, A.; Liu, S.; Zubieta, J. *Inorg. Chem.* **1990**, *29*, 2549–2551.
(37) Karlin, K. D.; Gan, Q.-f.; Tyeklár, Z. *Chem. Commun.* **1999**, 2295–2296.
(38) Frey, S. T.; Sun, H. H. J.; Murthy, N. N.; Karlin, K. D. *Inorg. Chim. Acta* **1996**, *242*, 329–338.
(39) Walsdorff, C.; Park, S.; Kim, J.; Heo, J.; Park, K.-M.; Oh, J.; Kim, K. *J. Chem. Soc., Dalton Trans.* **1999**, 923–929.
(40) Ohi, H.; Tachi, Y.; Itoh, S. *Inorg. Chem.* **2006**, *45*, 10825–10835.
(41) Ohi, H.; Tachi, Y.; Itoh, S. *Inorg. Chem.* **2004**, *43*, 4561–4563.
(42) Brown, E. C.; Johnson, B.; Palavicini, S.; Kucera, B. E.; Casella, L.; Tolman, W. B. *Dalton Trans.* **2007**, 3035–3042.
(43) Battaini, G.; Granata, A.; Monzani, E.; Gullotti, M.; Casella, L. *Adv. Inorg. Chem.* **2006**, 185–233.
(44) Adams, H.; Bailey, N. A.; Dwyer, J. S.; Fenton, D. E.; Hellier, P. C.; Hempstead, P. D.; Latour, J. M. *J. Chem. Soc., Dalton Trans.* **1993**, 1207–1216.
(45) Chen, P. P. Y.; Yang, R. B. G.; Lee, J. C. M.; Chan, S. I. *Proc. Nat. Acad. Sci.* **2007**, *104*, 14570–14575.
(46) Ghiladi, R. A. Thesis, Johns Hopkins University, 2003.

Chart 1

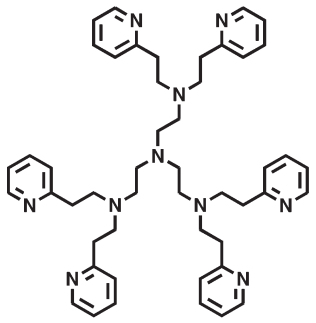

Karlin, K. D. & coworkers

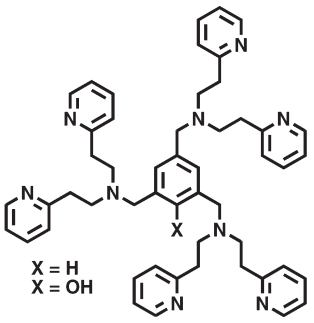

Karlin, K. D. & coworkers

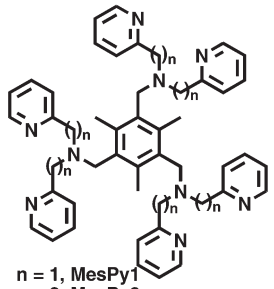

Karlin, K. D. & coworkers

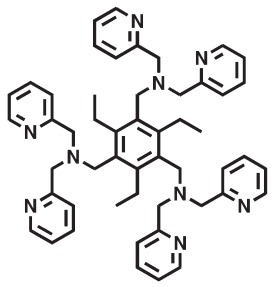

Kim, K. & coworkers

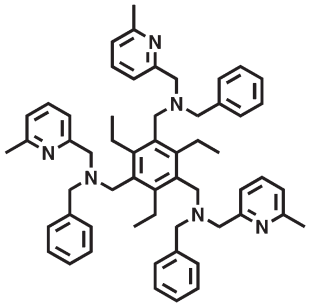

Itoh, S. & coworkers

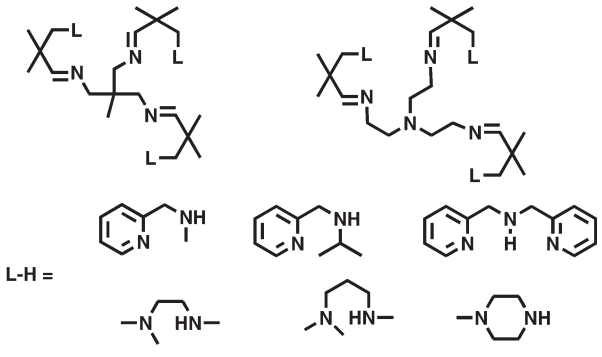

Tolman, W. B. & coworkers

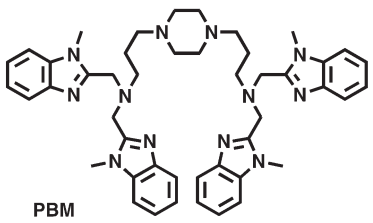

Casella, L. & coworkers

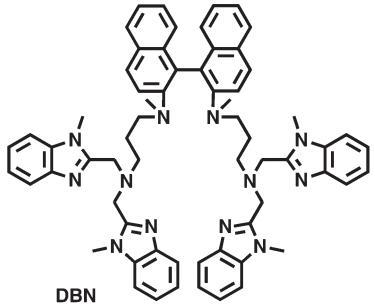

Casella, L. & coworkers

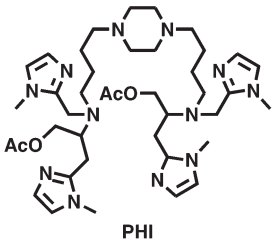

Casella, L. & coworkers

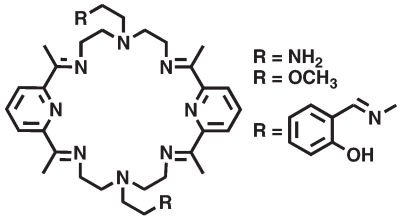

Fenton, D. E. & coworkers

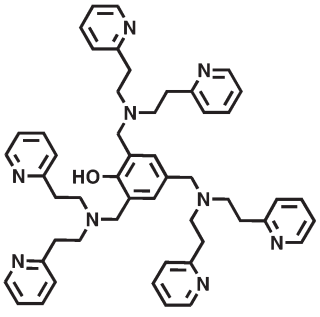

Karlin, K. D. & coworkers

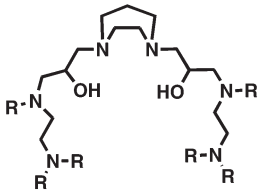

Chan S. I. & coworkers

three copper centers to be on the same side of the mesityl plane.[39−41]

In this report, we present our continuing efforts toward modeling the active sites of the multicopper enzymes by use of a ligand scaffold based upon the bowl-shaped cyclotriveratrylene (CTV) molecule[47] possessing appended pyridyl alkylamine moieties.[46] The hope was that the more structured CTV architecture[47−51] will help promote close di- or

(47) Collet, A. *Tetrahedron* **1987**, *43*, 5725–5759.

(48) Zhang, S.; Echegoyen, L. *J. Am. Chem. Soc.* **2005**, *127*, 2006–2011.

(49) Ameijde, J. v.; Liskamp, R. M. J. *Org. Biomol. Chem.* **2003**, *1*, 2661–2669.

(50) Bohle, D. S.; Stasko, D. J. *Inorg. Chem.* **2000**, *39*, 5768–5770.

(51) vanStrijdonck, G. P. F.; vanHaare, J. A. E. H.; Honen, P. J. M.; vandenSchoor, R. C. G. M.; Feiters, M. C.; vanderLinden, J. G. M.; Steggerda, J. J.; Nolte, R. J. M. *J. Chem. Soc., Dalton Trans.* **1997**, 449–461.

tricopper interactions as occur in the multicopper enzyme active sites. Investigations of dioxygen reactivity with mono- and binuclear copper(I) complexes employing similar tetradentate pyridyl-alkylamine copper chelates have been previously carried out,[5,6,9,52−54] thereby establishing patterns for copper-dioxygen adduct formation and representing a good starting point for obtaining insights with the CTV ligand and achieving our current objectives.

Experimental Section

Materials and Methods. Unless otherwise stated all solvents and chemicals used were of commercially available analytical grade. Methanol, dichloromethane, acetonitrile (CH_3CN), tetrahydrofuran (THF), pentane, 2-methyltetrahydrofuran (Me-THF), acetone, and diethyl ether were used after passing them through a 60 cm long column of activated alumina (Innovative Technologies, Inc.) under argon. Preparative thin-layer chromatography was performed on a Harrison Research Chromatotron Model 8924 equipped with a 4 mm Adsorbosil-Plus P (silica gel, Alltech Associates) plate. Thin-layer chromatography was performed on "Baker-Flex" aluminum oxide (IB-F) and silica gel (IB2-F) plates (J. T. Baker). Alumina (EM-Science, AX-0612, 80−200 mesh) and silica gel 60 (EM-Science, 7734, 70−230 mesh) were also purchased from commercial sources. All ligands were synthesized and characterized in the air unless otherwise stated. Preparation and handling of air-sensitive materials were carried out under an argon atmosphere using standard Schlenk techniques. Solvents and solutions were deoxygenated by either repeated freeze−pump−thaw cycles (5×), or by bubbling of argon (> 25 min.) directly through the solution. Solid samples were stored and transferred in an MBraun LabMaster 130 inert atmosphere (< 1 ppm O_2, < 1 ppm H_2O) glovebox under nitrogen atmosphere. NMR spectra were measured on either a Varian NMR instrument at 400 MHz or a Bruker 400 MHz spectrometer. All spectra were recorded in 5 mm-o.d. NMR tubes, and chemical shifts were reported as δ values downfield from an internal standard of Me_4Si (^1H). EI and FAB mass spectra were obtained using a VG70S instrument. ESI mass spectra were acquired using a Finnigan LCQDeca ion-trap mass spectrometer equipped with an electrospray ionization source (Thermo Finnigan, San Jose, CA). Samples were dissolved in CH_3OH and introduced into the instrument at a rate of 10 μL/min using a syringe pump via a silica capillary line. The heated capillary temperature was 250 °C, and the spray voltage was 5 kV. X-band electron paramagnetic resonance (EPR) spectra were recorded on a Bruker EMX CW-EPR spectrometer controlled with a Bruker ER 041 XG microwave bridge operating at X-band (~9.472 GHz). The low temperature experiments were carried out in tetrahydrofuran (THF) at 77 K using a $N_2(l)$ finger dewar flask. UV−vis spectra were recorded with either a Cary-50 Bio spectrophotometer equipped with a fiber optic coupler (Varian) and a fiber optic dip probe (Hellma: 661.302-QX-UV-2 mm-for-low-temperature) or a Hewlett-Packard Model 8453A diode array spectrophotometer equipped with a two-window quartz H.S. Martin Dewar filled with cold MeOH (25 °C to −85 °C) which was maintained and controlled by a Neslab VLT-95 low temp circulator. Spectrophotometer cells used were made by Quark Glass with column and pressure/vacuum side stopcock and 2 mm path length. The copper(I) complex used for low temperature UV−vis and all reactivity studies reported below are the ClO_4^- and $B(C_6F_5)_4^-$ salt complexes unless otherwise stated. ***Caution!*** *While we have experienced no problems in working with perchlorate compounds, they are potentially explosive and care must be taken not to work with large quantities*. Dioxygen was dried by passing through a short column of supported P_4O_{10} (Aquasorb, Mallinckrodt) and was bubbled into reaction solutions via an 18-gauge, 24 inch-long stainless steel syringe needle. IR spectra were collected using a Mattson Instruments Galaxy series FT-IR (model 4030) that was controlled by the PC program WinFIRST. Elemental analyses were performed by Desert Analytics (Tucson, AZ).

4-(2-Propenyloxy)-3-methoxybenzyl Alcohol. To a flame-dried 3-neck 2000 mL round-bottom flask equipped with a stir bar and reflux condenser were added in the following order: anhydrous K_2CO_3 (225.0 g, 1.628 mol), 4-hydroxy-3-methoxybenzyl alcohol (200.0 g, 1.297 mol), 1000 mL of acetone, and allyl bromide (130 mL, 1.502 mol). The resulting yellow solution was refluxed under argon for 18 h. After cooling to room temperature (RT), the solvent was reduced in vacuo to give a yellow solid, after which 1000 mL of dichloromethane was added. The solution was extracted with water (2 × 750 mL), brine (1 × 750 mL), dried over anhydrous Na_2SO_4, filtered, and the resulting solution was concentrated in vacuo to give a light yellow solid. Recrystallization of the crude material by dissolving in 600 mL of boiling 2:1 diisopropyl/diethyl ethers and subsequent cooling to 0 °C yielded 4-(2-propenyloxy)-3-methoxybenzyl alcohol (152.0 g, 783 mmol) as a white solid in 60.3% yield. ^1H NMR ($CDCl_3$): δ 3.89 (s, 3H, OCH_3), 4.62 (m, br, OCH_2 and OH), 5.28 (d, 1H, J = 10.5 Hz, allylic H), 5.40 (d, 1H, J = 17.3 Hz, allylic H), 6.09 (m, 1H, allylic H), 6.85−6.94 (m, 3H, Ar H).

(±)2,7,12-Trimethoxy-3,8,13-tris(2-propenyloxy)-10,15-dihydro-5*H*-tribenzo[*a*,*d*,*g*]cyclononene. To a 3-neck 2000 mL round-bottom flask equipped with a stir bar and containing 1250 mL of methanol solvent was added 4-(2-propenyloxy)-3-methoxybenzyl alcohol (152.0 g, 783 mmol), yielding a light yellow solution. Upon cooling to 0 °C, 70% perchloric acid (600 mL) was added dropwise over a period of 1 h. The resulting red solution was allowed to warm to RT, after which a white precipitate formed. After stirring for an additional 18 h, dichloromethane (1500 mL) was added to quench the reaction, and the dark red organic layer was collected and washed with water (4 × 1000 mL), brine (2 × 750 mL), dried over Na_2SO_4, and filtered. The red-brown solution was then concentrated in vacuo to give a sticky red-brown solid, to which 800 mL of diethyl ether was added and the mixture stirred. Filtration of the cloudy red-brown solution gave (±) 2,7,12-trimethoxy-3,8,13-tris(2-propenyloxy)-10,15-dihydro-5*H*-tribenzo[*a*,*d*,*g*]cyclononene (57.3 g, 108 mmol) as a white solid in 41.5% yield. ^1H NMR ($CDCl_3$): δ 3.52 (d, 3H, J = 13.8H, H_{eq}), 3.83 (s, 9H, OCH_3), 4.58 (s, br, 6H, OCH_2), 4.74 (d, 3H, J = 13.8 Hz, H_{ax}), 5.25 (d, 3H, J = 10.5 Hz, allylic H), 5.37 (d, 3H, J = 17.3 Hz, allylic H), 6.06 (m, 3H, allylic H), 6.79 (s, 3H, H1), 6.85 (s, 3H, H2).

(±)2,7,12-Trimethoxy-3,8,13-trihydroxy-10,15-dihydro-5*H*-tribenzo[*a*,*d*,*g*]cyclononene (Cyclotriguaiacylene, CTG). To a 3-neck 2000 mL round-bottom flask equipped with a stir bar and a reflux condenser was added in the following order: (±) 2,7,12-trimethoxy-3,8,13-tris(2-propenyloxy)-10,15-dihydro-5-*H*-tribenzo[*a*,*d*,*g*]cyclo-nonene (57.3 g, 108 mmol), 600 mL of acetonitrile, 180 mL of water, triethylammonium formiate (60.0 g, 410 mmol), triphenylphosphine (PPh_3, 2.03 g, 7.740 mmol), and a catalytic amount of palladium(II) acetate (250 mg, 1.110 mmol). The cloudy yellow mixture was refluxed for 4 h, after which the acetonitrile was removed via rotary evaporation, and 1500 mL of ethyl acetate was added. The organic layer was filtered, washed with water (2 × 1000 mL), brine (1 × 1000 mL), dried over Na_2SO_4, and again filtered. Concentration resulted in a pale green-yellow solid to which some diethyl ether was added and stirred. Isolation of the CTG (21.0 g, 51.4 mmol) by filtration gave an off-white solid in 47.6% yield.

(52) Maiti, D.; Woertink, J. S.; Vance, M. A.; Milligan, A. E.; Narducci Sarjeant, A. A.; Solomon, E. I.; Karlin, K. D. *J. Am. Chem. Soc.* **2007**, *129*, 8882–8892.

(53) Zhang, C. X.; Kaderli, S.; Costas, M.; Kim, E.-i.; Neuhold, Y.-M.; Karlin, K. D.; Zuberbühler, A. D. *Inorg. Chem.* **2003**, *42*, 1807–1824.

(54) Karlin, K. D.; Kaderli, S.; Zuberbühler, A. D. *Acc. Chem. Res.* **1997**, *30*, 139–147.

^{1}H NMR ($CDCl_3$): δ 3.48 (d, 3H, J = 13.7 Hz, H_{eq}), 3.84 (s, 9H, OCH_3), 4.69 (d, 3H, J = 13.7 Hz, H_{ax}), 6.81 (s, 3H, H1), 6.86 (s, 3H, H2). EI[+] MS: (m + H^+): m/z 408.

(±) **2,7,12-Trimethoxy-3,8,13-tris((2-(6-chloromethyl) pyridyl)-methyoxy)-10,15-dihydro-5*H*-tribenzo[*a*,*d*,*g*]cyclononene (CTV-Halide).** To a flame-dried 2-neck 500 mL round-bottom flask equipped with a stir bar and rubber septum was added in the following order under argon: K_2CO_3 (5.0 g, 36.1 mmol), 200 mg of KI, 500 mg of Bu_4NI, CTG (1.5 g, 3.68 mmol), 2,6-bis-(chloromethyl)pyridine (6.0 g, 34.1 mmol), and 200 mL of high-purity acetone. The cloudy yellow reaction mixture was stirred at RT under argon for 5 h, after which an additional amount of 2,6-bis(chloromethyl)pyridine (6.0 g, 34.1 mmol) dissolved in 75 mL of acetone was added under argon flow. After an additional 65 h of stirring at ambient temperature, the reaction mixture was filtered, and the filtrate was concentrated in vacuo. The resulting yellow solid was dissolved in 500 mL of dichloromethane, and the clear yellow solution was washed with water (2 × 500 mL), brine (1 × 500 mL), dried over Na_2SO_4, filtered, and reduced via rotary evaporation to give a yellow solid. The crude material was applied to a silica column (80−200 mesh, 4.0 cm. o.d. × 18.0 cm.) where excess 2,6-bis(chloromethyl)pyridine was eluted with dichloromethane. Acetone was then allowed to pass down the column, thereby eluting the partially purified CTV-halide product. After concentration, the off-white solid material was further purified using a Chromatotron (eluent: 1.5% EtOH in CH_2Cl_2). Removal of solvent yielded CTV-halide (1.88 g, 2.27 mmol) as a white solid in 62% yield. TLC (silica, 1.5% CH_3OH in CH_2CL_2) Rf: 0.30. ^{1}H NMR ($CDCl_3$): δ 3.43 (d, 3H, J = 13.8 Hz, H_{eq}), 3.74 (s, 9H, OCH_3), 4.67 (d, 3H, J = 13.8 Hz, H_{ax}), 4.68 (s, 6H, CH_2Cl), 5.24 (s, 6H, OCH_2), 6.68 (s, 3H, H1), 6.81 (s, 3H, H2), 7.38 (d, 3H, J = 7.80 Hz, Ar H), 7.46 (d, 3H, J = 7.80 Hz, Ar H), 7.71 (t, 3H, J = 7.80 Hz, Ar H). FAB MS (m + H^+): m/z 826.

(±) **2,7,12-Trimethoxy-3,8,13-tris(6-(tris((2-pyridyl)methyl)amine)-methoxy)-10,15-dihydro-5*H*-tribenzo[*a*,*d*,*g*]cyclononene (CTV-TMPA).** To a flame-dried 2 neck 250 mL round-bottom flask equipped with a stir bar was added in the following order under argon: K_2CO_3 (5.0 g, 36.1 mmol), tetrabutylammmonium iodide (2.5 g, 6.78 mmol), bis(2-picolyl)amine (2.5 g, 12.6 mmol), 125 mL of distilled acetonitrile, diisopropylethylamine (2.5 mL, 14.4 mmol), and CTV-halide (1.2 g, 1.45 mmol). The reaction mixture was heated to 35 °C and allowed to stir at this temperature under inert atmosphere overnight. Then, the solvent was removed via rotary evaporation and the yellow-brown oil was dissolved in 500 mL of dichloromethane, washed with water (2 × 500 mL), brine (1 × 500 mL), dried over Na_2SO_4 and filtered. To this clear yellow solution was added phthalic anhydride (2.24 g, 15.1 mmol), and the reaction mixture was allowed to stir under argon for two additional hours. The solution was then washed with 1 N NaOH (3 × 500 mL), brine (1 × 500 mL), dried over Na_2SO_4, filtered, and the solvent removed in vacuo to give dark yellow oil. Upon dissolving the oil in 10 mL of ethyl acetate, a white crystalline precipitate was formed. This precipitate was removed via filtration, and the resulting clear dark yellow solution was applied to an alumina column (unactivated, 80−200 mesh, 4.0 cm. o.d. × 18 cm.) and eluted with 3% CH_3OH in EtOAc. Removal of solvent gave CTV-TMPA (900 mg, 0.68 mmol) as an off-white solid in 47% yield. TLC (alumina, 3% CH_3OH in EtOAc) Rf: 0.30−0.35. ^{1}H NMR ($CDCl_3$): δ 3.39 (d, 3H, J = 13.7 Hz, H_{eq}), 3.63 (s, 9H, OCH_3), 3.89 (s, br, 18H, NCH_2), 4.63 (d, 3H, J = 13.7 Hz, H_{ax}), 5.20 (s, 6H, OCH_2), 6.63 (s, 3H, H1), 6.80 (s, 3H, H2), 7.13−7.68 (m, 27H, Ar H), 8.53 (d, 6H, J = 4.2 Hz, Ar H). FAB MS (m + H^+): m/z 1316. Anal. Calcd For $C_{81}H_{78}N_{12}O_6$: C, 73.95; H, 5.98; N, 12.78. Found: C, 73.60; H, 5.56; N, 11.68. Assignments of H_{ax} and H_{eq} peaks were carried out following literature reports.[55,56]

[(CTV-TMPA)Cu^I_3](ClO_4)$_3$. In a 25 mL Schlenk flask equipped with a stir bar was added under argon CTV-TMPA (300 mg, 0.23 mmol) and [$Cu(CH_3CN)_4$](ClO_4) (220 mg, 0.69 mmol). Addition of 10 mL of deoxygenated acetonitrile resulted in a yellow solution, which was allowed to stir under inert atmosphere for 30 min. Deoxygenated diethylether was added until the solution began to turn cloudy, at which point the yellow solution was passed through a coarse porosity Schlenk filter frit into a 100 mL air-free flask. Further addition of deoxygenated diethyl ether (75 mL), followed by vigorous stirring, led to the formation of a yellow precipitate. The clear mother liquor was decanted under a flow of argon, and the precipitate was washed with 80 mL of deoxygenated diethyl ether. After filtration under argon, the yellow solid was placed under vacuum for 2 h which resulted in a free-flowing solid (295 mg, 72% yield). ^{1}H NMR (CD_3CN): δ 3.61 (d, 3H, J = 13.5 Hz, H_{eq}), 3.72 (s, 9H, OCH_3), 3.96 (s, br, 18H, NCH_2), 4.82 (d, 3H, J = 13.4 Hz, H_{ax}), 5.30 (dd, 6H, J = 12.6 and 31.8 Hz, OCH_2), 7.00 (s, 3H, H1), 7.15 (s, 3H, H2), 7.29−7.77 (m, 27H, Ar H), 8.51 (s, 6H, Ar H).

[(CTV-TMPA)Cu^I_3]($B(C_6F_5)_4$)$_3$ (1). CTV-TMPA (0.250 g, 0.190 mmol) and [$Cu^I(CH_3CN)_4$]$B(C_6F_5)_4$[57] (0.172 g, 0.190 mmol) were placed in a 25 mL Schlenk flask under argon. THF (2 mL) was added under argon to the mixture of solids to form a light yellow solution. The resulting solution was stirred under argon for 30 min. Pentane (14 mL) was then added to the solution to precipitate a light yellow solid. The supernatant was decanted, and the solid was recrystallized three times from THF/pentane under argon and dried under vacuum (1 h), giving 0.458 g of light yellow powder (68% yield). Anal. Calcd For $C_{153}H_{78}B_3Cu_3F_{60}N_{12}O_6$: C, 51.86; H, 2.22; N, 4.74. Found: C, 51.58; H, 2.92; N, 4.10.

Electrochemistry. Cyclic voltammetry was carried out with a Bioanalytical Systems BAS-100B electrochemistry analyzer. The sample cell used was a standard three-electrode system with platinum wire auxiliary as the counter electrode. A glassy carbon electrode (GCE, BAS MF 2012) was used as the working electrode. The reference electrode was Ag/Ag^+. Dimethylformamide (DMF) as solvent was deoxygenated by argon bubbling. The measurements were performed at RT in DMF containing 0.1 M tetrabutylammonium hexafluorophosphate (TBAHP) and 1−0.1 mM copper complex.

Reaction of [(CTV-TMPA)Cu^I_3]($B(C_6F_5)_4$)$_3$ (1) with [$Fe^{III}Cp_2$]$^+$. Complex [(CTV-TMPA)Cu^I_3]($B(C_6F_5)_4$)$_3$ (**1**) (0.020 g, 0.006 mmol) was dissolved in 3.0 mL of THF and taken in a UV−vis cuvette inside the inert atmosphere box. On the benchtop, an initial spectrum was recorded. In a separate 5 mL Schlenk flask in the glovebox, [$Fe^{III}Cp_2$]PF_6 (Aldrich; 0.050 g, 0.151 mmol) was dissolved in 0.5 mL of degassed THF. A total of 56 μL (0.017 mmol) of the THF solution of [$Fe^{III}Cp_2$]PF_6 was added in the course of 5 min (~9 μL each time) via microliter syringe to the copper(I) solution **1**. The solution was purged with Ar after each addition of ferrocinium ion and a UV−vis spectrum recorded. An EPR of this solution was recorded. EPR (9.471 GHz, MeTHF, 77K): $g_\parallel$ = 2.246, $g_\perp$ = 2.046, $A_\parallel$ = 152 G, $A_\perp$ = 29.3 G. The EPR of the previously reported crystallographically characterized [{(L^{CH_2OMe})Cu^{II}(Cl)}$_2$]($B(C_6F_5)_4$)$_2$[95] (0.180 g, 0.080 mmol) complex in 3.1 mL of THF was compared with the above EPR of the fully oxidized **1** under similar experimental conditions. In a separate UV−vis cuvette, similar experiments were carried out, and the addition of 1 more equiv of [$Fe^{III}Cp_2$]$^+$ solution did not cause further UV−vis or EPR spectral changes.

[(CTV-TMPA)Cu^{II}_3(Cl)$_3$]($B(C_6F_5)_4$)$_3$ (1-Cl). [(CTV-TMPA)Cu^I_3]($B(C_6F_5)_4$)$_3$ (**1**) (0.080 g, 0.023 mmol) was placed in a

(55) Collet, A.; Gabard, J. *J. Org. Chem.* **1980**, *45*, 5400–5401.
(56) Canceill, J.; Collet, A.; Gottarelli, G. *J. Am. Chem. Soc.* **1984**, *106*, 5997–6003.
(57) Liang, H.-C.; Kim, E.; Incarvito, C. D.; Rheingold, A. L.; Karlin, K. D. *Inorg, Chem.* **2002**, *41*, 2209–2212.

25 mL Schlenk flask under argon. Six drops of degassed $CHCl_3$ were added to THF (2.0 mL, degassed) and the solvent mixture was added to the copper(I)-complex containing flask. Under argon, the mixture was stirred for 3 h while the solution turned to green. Pentane (15 mL, degassed) was then added to precipitate a solid. The copper complex obtained was further recrystallized three times from THF/pentane and dried under vacuum (2 h), giving 0.053 g of light yellow powder (64% yield). EPR (9.471 GHz, THF, 77 K): $g_{\|} = 2.23$, $g_{\perp} = 2.05$, $A_{\|} = 143$ G, $A_{\perp} = 33.5$ G. Anal. Calcd For $[(CTV\text{-}TMPA)Cu^{II}{}_3(Cl)_3](B(C_6F_5)_4)_3$ (**1-Cl**), $C_{153}H_{78}B_3Cl_3Cu_3F_{60}N_{12}O_6$: C, 50.35; H, 2.15; N, 4.61. Found: C, 50.16; H, 2.12; N, 4.32. A cyclic voltammetry study and ESI-MS analysis (with the perchlorate salt) were also carried out.

Generation of Copper−Carbonyl Complex from the Reaction of CO and 1: Quantitative Measurement of the Release of CO upon Addition of PPh_3. Bubbling CO through a THF solution of $[(CTV\text{-}TMPA)Cu^{I}{}_3](B(C_6F_5)_4)_3$ (**1**) generates the corresponding carbonyl adduct $[(CTV\text{-}TMPA)Cu^{I}{}_3(CO)_3](B(C_6F_5)_4)_3$ (**1-CO**). IR spectroscopy: $\nu_{CO} = 2094$ cm^{-1}. ^{1}H NMR (DMSO): δ 3.56 (d, 3H, H_{eq}), 3.75 (s, 9H, OCH_3), 4.2 (s, br, 18H, NCH_2), 4.86 (d, 3H, H_{ax}), 5.37 (6H, OCH_2), 7.14 (s, 3H, H1), 7.31 (s, 3H, H2), 7.36−7.89 (m, 27H, Ar H), 8.55 (s, 6H, Ar H). Anal. Calcd For $[(CTV\text{-}TMPA)Cu^{II}{}_3(CO)_3](B(C_6F_5)_4)_3$ (**1-CO**), $C_{156}H_{78}B_3Cu_3F_{60}N_{12}O_9$: C, 51.65; H, 2.17; N, 4.63. Found: C, 51.44; H, 2.54; N, 4.13.

To confirm that all three copper(I) sites bind CO, PPh_3 was added to **1-CO** and the CO release was quantitated. In a drybox, $[(CTV\text{-}TMPA)Cu^{I}{}_3](B(C_6F_5)_4)_3$ (0.0025 g, 0.0007 mmol) was dissolved in 10 mL of THF within a UV−vis cuvette. Out on a benchtop, the cuvette was cooled to −90 °C in the cooling Dewar flask of the UV−vis instrument. Carbon monoxide was bubbled through the solution for ∼5 s and excess CO was removed completely via 5 vacuum/argon cycles. Also, inside a drybox within a separate 5 mL Schlenk flask, PPh_3 (0.0055 g, 0.020 mmol) was dissolved in 1 mL of degassed THF. A total of a 100 μL (0.0020 mmol) of PPh_3 solution was added via microliter syringe to the UV−vis cuvette containing the solution of **1-CO**. A 100 μL solution of $(F_8TPP)Fe^{II}(THF)_2$ {F_8-TPP = tetrakis(2,6-difluorophenyl)porphyrinate(2-)} (0.0018 g, 0.021 mmol) was added via a microliter syringe to the resulting solution. UV−vis spectrum of this final solution was recorded and was compared with the UV−vis spectrum generated from a separate solution of $[(F_8TPP)Fe^{II}(THF)_2]$ (0.0018 g, 0.021 mmol) in 10.2 mL of THF which had been bubbled with CO. A ∼2.9 equiv of CO removal upon addition of 3 equiv of PPh_3 to one equiv of **1-CO** was observed.

Reaction of $[(CTV\text{-}TMPA)Cu^{I}{}_3](B(C_6F_5)_4)_3$ (1) with O_2. A 3.0 mL of THF solution of **1** (0.015 g, 0.0042 mmol) was taken in a UV−vis cuvette assembly under argon; this was cooled to −80 °C, and an initial UV−vis spectrum was recorded. Dioxygen was bubbled for 30 s through the solution using a long syringe needle, and the new spectrum recorded upon removal of excess O_2. The deep purple product is formulated as **1-O_2** (see Discussion).

Thermal Transformation Product of 2-O_2. $[(CTV\text{-}TMPA)Cu^{I}{}_3](B(C_6F_5)_4)_3$ (**1**) (0.009 g, 0.0025 mmol) was dissolved in 4.0 mL of THF and transferred to a UV−vis cuvette assembly inside the MBraun glovebox. Outside on the benchtop, the cuvette was cooled to −80 °C and an initial spectrum was recorded. Dioxygen was bubbled through the solution with a long syringe needle. This results in an immediate color change from colorless to deep purple (excess dioxygen removed). The UV−vis spectra were recorded at −80 °C with respect to time.

In a separate 25 mL Schlenk flask, $[(CTV\text{-}TMPA)Cu^{I}{}_3](B(C_6F_5)_4)_3$ (**1**) (0.044 g, 0.012 mmol) was dissolved in 2 mL of THF, and O_2 was bubbled through the solution upon cooling to −80 °C. This was allowed to warm to RT, and then pentane (20 mL) was then added to precipitate an intensely purple solid. The copper complex obtained was further recrystallized four times from THF/pentane and dried under vacuum (4 h), giving 0.033 g of a dark purple powder (76% yield). Anal. Calcd For $[(CTV\text{-}TMPA)Cu^{II}{}_3(OH)_3](B(C_6F_5)_4)_3$ (**1-Dec**), $C_{153}H_{81}B_3Cu_3F_{60}N_{12}O_9$: C, 51.13; H, 2.27; N, 4.68. Found: C, 50.95; H, 2.37; N, 5.15. Note, however, that the IR spectrum (Nujol mull) did not reveal an expected O−H stretch in the 3400−3700 cm^{-1} region. An EPR spectrum showed a single broad isotropic signal, see the Supporting Information. We did not attempt to obtain mass spectrometric data.

Synthesis of $[(CTV\text{-}TMPA)Cu^{I}{}_3(PPh_3)_3](B(C_6F_5)_4)_3$ (1-PPh_3). A 1.5 mL of THF solution of $[(CTV\text{-}TMPA)Cu^{I}{}_3](B(C_6F_5)_4)_3$ (**1**) (0.067 g, 0.019 mmol) was taken in a 25 mL Schlenk flask, and PPh_3 (0.015 g, 0.058 mmol) was added (100 μL THF) anaerobically via a microliter syringe. The resulting solution was stirred under argon for 20 min. Pentane (15 mL) was then added to the solution to precipitate a white solid. The supernatant was decanted, and the solid was recrystallized four times from THF/pentane under argon and dried under vacuum (3 h), giving 0.068 g of white powder (84% yield). Anal. Calcd For $[(CTV\text{-}TMPA)Cu^{I}{}_3(PPh_3)_3](B(C_6F_5)_4)_3$ (**1-PPh_3**), $C_{207}H_{123}B_3Cu_3F_{60}N_{12}O_6P_3$: C, 57.42; H, 2.86; N, 3.88. Found: C, 57.61; H, 3.01; N, 3.51. ^{1}H NMR (DMSO): δ 3.49 (d, 3H, H_{eq}), 3.56−4.33 (m, 27H, OCH_3 and NCH_2), 4.76 (d, 3H, H_{ax}), 5.04 (6H, OCH_2), 7.01 (s, 3H, H1), 7.10 (s, 3H, H2), 7.19−7.91 (m, 42H, Ar H), 8.42 (s, 6H, Ar H).

^{31}P NMR Study of $[(CTV\text{-}TMPA)Cu^{I}{}_3(PPh_3)_3](B(C_6F_5)_4)_3$ (1-PPh_3). Inside the glovebox, $[(CTV\text{-}TMPA)Cu^{I}{}_3(PPh_3)_3](B(C_6F_5)_4)_3$ (**1-PPh_3**) (0.014 g, 0.0032 mmol) and $P(Mes)_3$ (0.0034 g, 0.0098 mmol) was taken into a NMR sample tube and was dissolved in degassed d_8-THF. Out on the benchtop, with a rubber septum on top to maintain anaerobic conditions, a ^{31}P NMR was recorded. ^{31}P NMR (d_8-THF): δ 3.79 (3P, **1-PPh_3**), −35.92 (3.093 P, $PMes_3$).

Generation of Disulfido-Dicopper(II) Complex, $[\{(CTV\text{-}TMPA)Cu^{II}{}_3\}_2(\mu\text{-}1,2\text{-}S_2{}^{2-})_3]^{6+}$ (1-S). $[(CTV\text{-}TMPA)Cu^{I}{}_3](B(C_6F_5)_4)_3$ (**1**) (0.0192 g, 0.0054 mmol) was dissolved in 3.8 mL of THF under argon in a UV−vis cuvette with a glass stopper. Solid elemental sulfur (0.0017 g) was dissolved in 0.5 mL of THF upon stirring in a 5 mL Schlenk flask under argon. This sulfur containing solution was cooled to −80 °C using an acetone/dry ice bath. The glass stoppers from the cuvette and the flask were interchanged for rubber septa. From the stock solution, 50 μL of the sulfur containing solution (0.0053 mmol) was added to the solution in the cuvette. Purging argon for 5 s caused thorough mixing of sulfur solution with the copper(I) solution. The resulting solution was kept at −80 °C for 5 min, and a UV−vis spectrum was recorded. Three further additions of the sulfur solution (50 μL each time) accompanied by Ar bubbling and recording of UV−vis spectra after 10 min were carried out. Further addition of sulfur solution did not cause any observable UV−vis change. A nice purple colored solution ($\lambda_{max} = 544$ nm) fully formed, designated as complex **1-S** (See Results and Discussion). Species **1-S** is stable at −80 °C; upon warming to RT it loses its UV−vis intensity, whereas based on the UV−vis changes recooling to −80 °C (under Ar) results in complete reformation of **1-S**. A blackish-purple colored copper complex was generated upon warming the −80 °C **1-S** solution to RT. This solution was filtered with Whatman filter paper (Glass Microfiber Filters, GF/C, Circles, 24 mm Ø, Catalog No. 1822024) plugged in pipet under argon, and the filtration was repeated five times with a new filter paper each time to confirm absolute removal of unreacted (or released upon warming) elemental sulfur from the reaction solution. A pentane solution (20 mL) was added to precipitate the copper product which was further recrystallized four times from THF/pentane under argon and then dried under vacuum (6 h). Anal. Calcd For $[(CTV\text{-}TMPA)Cu_3S_3](B(C_6F_5)_4)_3$: $C_{153}H_{78}B_3Cu_3F_{60}N_{12}O_6S_3$; C, 50.49; H, 2.16; N, 4.62; S, 2.64. Found: C, 49.26; H, 2.29; N, 4.11; S, 3.3. The high S and low C and N content, despite

many recrystallizations (with filtration), may indicate the presence of some polysulfane complex impurities.

Resonance Raman (rR) Spectroscopy. rR spectroscopic measurements were undertaken using a Princeton Instruments ST-135 back-illuminated CCD detector on a Spex 1877 CP triple monochromator with 1200, 1800, and 2400 grooves/mm holographic spectrograph gratings. The excitation was provided by Coherent 190C−K Kr+ and Innova Sabre 25/7 Ar+ CW lasers. The spectral resolution was <2 cm^{-1}. Samples were prepared in standard low-grade NMR tubes. Sample concentrations were approximately 1.0 mM and 1.53 mM in copper for dioxygen reactivity. Sample concentrations were approximately 2.45 mM in copper for sulfur reactivity. All the samples were run at 77 K in a liquid N_2 finger Dewar (Wilmad).

The precursor copper(I) sample solutions were prepared in the glovebox in NMR tubes under N_2 and were cooled to −80 °C on the benchtop, after which O_2 bubbling was carried out via syringe. The solutions were frozen in liquid N_2 and sent to Stanford University for rR spectroscopic interrogation.

Results and Discussion

Synthesis of Cyclotriveratrylene (CTV) Based Trinucleating Ligand, CTV-TMPA. As mentioned, we designed this tripodal ligand system based on the building block cyclotriveratrylene (2,3,7,8,12,13-hexamethoxy-10,15-dihydro-5*H*-tribenzo[*a*,*d*,*g*] cyclononene) to promote close metal−metal interactions. This molecule has a rigid, bowl-like shape and possesses 3-fold symmetry. Functionalized CTV ligands have for example been previously used to provide subsite differentiation for [4Fe-4S] protein model compounds,[58] and this structural motif seems well-suited for metal-cluster modeling.[50,58−60]

The functionalization of the cyclotriveratrylene framework provides a chiral ligand system CTV-TMPA; the conformational inversion of their nine-membered ring is very slow at RT.[47] The CTV-TMPA ligand employs the TMPA {= tris(2-pyridylmethyl)amine} tetradentate copper chelate whose corresponding mononuclear Cu^I/O_2 chemistry is well established with respect to not only the types of dioxygen adducts possible but also their kinetics and thermodynamics of formation.[9,52−54] To append a copper binding site to the CTV periphery, it was determined that the best course of action was to proceed via functionalization of the cyclotriguaiacylene (CTG) precursor, which possesses a phenolic group ideal for nucleophilic substitution reactions (Scheme 1). We have previously demonstrated the ability to modify tetraarylporphyrins which contain meso-substituted 2-hydroxyphenyl arms with the copper-chelate TMPA {TMPA = tris(2-pyridylmethyl)amine},[61,62] and here we employed the same methodology and reaction conditions. The addition of 2,6-bis(chloromethyl)pyridine to CTG results in the formation of CTV-halide, whose alkylhalide functional group allows for the attachment of a variety of primary and secondary amines. We then chose bis(2-picolyl)amine for the synthesis of a trinucleating ligand, CTV-TMPA (Scheme 1).

Scheme 1

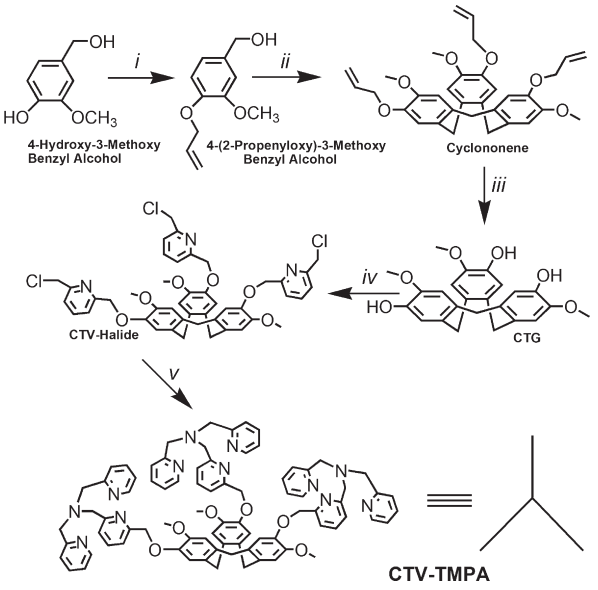

Scheme 2

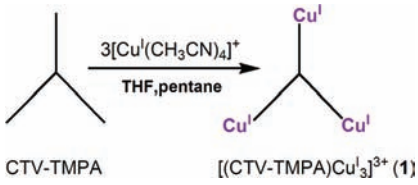

The successful generation of CTV-TMPA was confirmed by ^{1}H NMR spectroscopic analysis, FAB and ESI-MS spectrometry along with elemental analysis.

Synthesis and Characterization of a Tricopper(I) Complex. The light yellow tricopper(I) complex of CTV-TMPA, $[(\text{CTV-TMPA})Cu^I_3](B(C_6F_5)_4)_3$ (**1**) (Scheme 2), was generated by the addition of 3 equiv of $[Cu^I(CH_3CN)_4]B(C_6F_5)_4$ to 1 equiv of CTV-TMPA ligand in deoxygenated THF solvent under argon followed by precipitation with pentane. Isolation of a pure solid was achieved by recrystallization from THF/pentane. The copper(I) complex was also synthesized using the perchlorate (ClO_4^-) counteranion. The copper complexes $[(\text{CTV-TMPA})Cu^I_3]^{3+}$ (**1**) were characterized by elemental analysis and ^{1}H NMR spectroscopy, see Experimental Section.

Mononuclear Analogue for Copper Ion in CTV-TMPA. CTV-TMPA possesses three TMPA units in which one of the three pyridine rings of TMPA is 6−CH_2−O−R substituted and the three units are connected to a bowl-shaped cyclotriveratrylene moiety. We, previously, reported[52] the synthesis and characterization of the mono 6−CH_2−O−CH_3 substituted TMPA ligand, $\mathbf{L^{CH_2OMe}}$ (diagram) which is indeed a close mimic of any given mononuclear ligand portion of CTV-TMPA. X-ray structures of the copper complexes $[(\mathbf{L^{CH_2OMe}})Cu^I]^+$ (**2**), $[\{(\mathbf{L^{CH_2OMe}})Cu^{II}(Cl)\}_2]^{2+}$, and $[\{(\mathbf{L^{CH_2OMe}})Cu^{II}(Br)\}_2]^{2+}$ were described.[52] Several attempts to crystallize copper-complexes with CTV-TMPA were

(58) van Strijdonck, G. P. F.; van Haare, J. A. E. H.; Honen, P. J. M.; van den Schoor, R. C. G. M.; Feiters, M. C.; van der Linden, J. G. M.; Steggerda, J. J.; Nolte, R. J. M. *J. Chem. Soc., Dalton Trans.* **1997**, 449–461.
(59) Vériot, G.; Dutasta, J.-P.; Matouzenko, G.; Collet, A. *Tetrahedron* **1995**, *51*, 389–400.
(60) Matouzenko, G.; Veriot, G.; Dutasta, J. P.; Collet, A.; Jordanov, J.; Varret, F.; Perrin, M.; Lecocq, S. *New J. Chem.* **1995**, *19*, 881–885.
(61) Ghiladi, R. A.; Ju, T. D.; Lee, D.-H.; Moënne-Loccoz, P.; Kaderli, S.; Neuhold, Y.-M.; Zuberbühler, A. D.; Woods, A. S.; Cotter, R. J.; Karlin, K. D. *J. Am. Chem. Soc.* **1999**, *121*, 9885–9886.
(62) Ghiladi, R. A.; Karlin, K. D. *Inorg. Chem.* **2002**, *41*, 2400–2407.

Table 1. Cyclic Voltammetry Data for Copper(I) Complexes in DMF

complexes	$E_{1/2}$ (mV) vs Fc/Fc^+	ΔE_p (mV)	i_{pa}/i_{pc}
$[(TMPA)Cu^I(CH_3CN)]^+$ (**3**)	−610	80	0.80
$[(L^{CH_2OMe})Cu^I]^+$ (**2**)	−500	115	0.87
$[(CTV\text{-}TMPA)Cu^I_3]^{3+}$ (**1**)	−490	145	0.84

unsuccessful; thus we sought to produce evidence for tricopper binding and chemistry by chemical approaches.

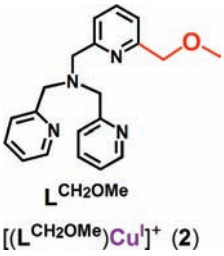

Electrochemistry. The half-wave potentials for the copper(I) complexes, $[(CTV\text{-}TMPA)Cu^I_3]^{3+}$ (**1**) and $[(L^{CH_2OMe})Cu^I]^+$ (**2**), were measured under argon in dimethylformamide (DMF) by cyclic voltammetry (CV). In DMF, **1** and **2** displayed a single quasi-reversible redox behavior with peak-current ratios of $i_{pa}/i_{pc} = 0.84$ and 0.87, respectively (Table 1). Peak separations were less than 150 mv at a scan rate of 100 mV/s. The ferrocene-ferrocinium couple under the same conditions showed $\Delta E_p = 85$ mV and $E_{1/2} = +55$ mV versus $Ag/AgNO_3$. A typical CV scan for $[(CTV\text{-}TMPA)Cu^I_3]^{3+}$ (**1**) is depicted in Figure 2.

The electrochemical behavior of $[(CTV\text{-}TMPA)Cu^I_3]^{3+}$ (**1**) can be explained by having the presence of three non-interacting copper ion centers where the redox process for each occurs at about the same potential. The appearance of only one CV wave has been previously reported for a number of multicopper systems.[63−66] Generally, one wave is seen if ΔE_p between two separate processes (i.e., $Cu^{II}-Cu^{II} + e^- \rightarrow Cu^{II}-Cu^I + e^- \rightarrow Cu^I-Cu^I$) is $< \sim 100-200$ mV. We have not attempted a more detailed analysis which might be used to estimate $E_{1/2}$ for the individual redox reactions;[63,67] however, this has been carried out in a number of cases.[65] In one example, for a triplatinum complex bound directly to the CTV catechol framework, Bohle and Stasko[68] observed three separate reversible redox couples, assigned as individual Pt-catecholate-to-Pt-seminquinoid species.

$[(CTV\text{-}TMPA)Cu^I_3]^{3+}$ (**1**) has very similar $E_{1/2}$ value (Table 1) to that of the close mononuclear mimic $[(L^{CH_2OMe})Cu^I]^+$ (**2**). These $E_{1/2}$ values are ∼110 mV more positive compared to the "parent" $[(TMPA)Cu^I(CH_3CN)]^+$ (**3**) complex which lacks a single 6-pyridyl substituent. Factors that can influence ligand-copper complex $E_{1/2}$ values include (i) the nature of chelating ligands, (ii) the donor atom types, and (iii) the geometry around tetra or pentacoordinate complexes.[5,7,69−71] A steric effect arises because of the $6-CH_2-O-R$ substituent (accompanied by a change of geometry) and is the likely cause of the positive shift in $E_{1/2}$ seen in $[(CTV\text{-}TMPA)Cu^I_3]^{3+}$ (**1**) and $[(L^{CH_2OMe})Cu^I]^+$ (**2**) relative to the parent $[(TMPA)Cu^I(CH_3CN)]^+$ (**3**) complex. Such suppositions come about from the study of similarly constructed ligand-copper systems.[72−74]

Figure 2. Cyclic voltammogram of $[(CTV\text{-}TMPA)Cu^I_3]^{3+}$ (**1**) in DMF at RT.

Scheme 3

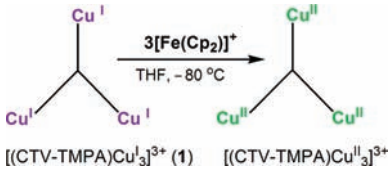

The ease of electrochemical oxidations of the three copper centers in $[(CTV\text{-}TMPA)Cu^I_3]^{3+}$ (**1**) correlates in a general way with the $[(L^{CH_2OMe})Cu^I]^+$ (**2**) reactivity with O_2, as described below. $[(CTV\text{-}TMPA)Cu^I_3]^{3+}$ (**1**) does react with O_2 at low temperature forming copper-dioxygen adducts. However, their tendency to give 1:1 and 2:1 adducts depends on geometric effects within the CTV architecture (vide infra).

Addition of 3 $[Fe^{III}Cp_2]^+$ to $[(CTV\text{-}TMPA)Cu^I_3]^{3+}$ (1). The tricopper(I) complex **1** can be oxidized to all copper(II) via addition of $[Fe^{III}Cp_2]^+$ as oxidant (Scheme 3). UV−vis absorption monitoring of solutions of $[(CTV\text{-}TMPA)Cu^I_3]^{3+}$ (**1**) after addition of $[Fe^{III}Cp_2]^+$ shows that 3 equiv are needed to complete the oxidation of **1**; after that, no further spectral changes are observed when further (i.e., excess) $[Fe^{III}Cp_2]^+$ is added (Figure 3). EPR spectra of the resulting fully oxidized copper species,

(63) Lee, D.-H.; Wei, N.; Murthy, N. N.; Tyeklár, Z.; Karlin, K. D.; Kaderli, S.; Jung, B.; Zuberbühler, A. D. *J. Am. Chem. Soc.* **1995**, *117*, 12498–12513.
(64) Karlin, K. D.; Tyeklár, Z.; Farooq, A.; Haka, M. S.; Ghosh, P.; Cruse, R. W.; Gultneh, Y.; Hayes, J. C.; Toscano, P. J.; Zubieta, J. *Inorg. Chem.* **1992**, *31*, 1436–1451.
(65) Oshio, H. *J. Chem. Soc., Dalton Trans.* **1990**, 2985–2989.
(66) Mazurek, W.; Bond, A. M.; O'Connor, M. J.; Wedd, A. G. *Inorg. Chem.* **1986**, *25*, 906–915.
(67) Richardson, D. E.; Taube, H. *Inorg. Chem.* **1981**, *20*, 1278.
(68) Bohle, D. S.; Stasko, D. *Chem. Commun.* **1998**, 567–568.
(69) Rorabacher, D. B. *Chem. Rev.* **2004**, *104*, 651–697.
(70) Hathaway, B. J. Copper. In *Comprehensive Coordination Chemistry*; Wilkinson, G., Ed.; Pergamon: New York, 1987; Vol. *5*, pp 533−774.
(71) Hatcher, L. Q.; Karlin, K. D. *Adv. Inorg. Chem.* **2006**, *58*, 131–184.
(72) Lucchese, B.; Humphreys, K. J.; Lee, D.-H.; Incarvito, C. D.; Sommer, R. D.; Rheingold, A. L.; Karlin, K. D. *Inorg. Chem.* **2004**, *43*, 5987–5998.
(73) Nagao, H.; Komeda, N.; Mukaida, M.; Suzuki, M.; Tanaka, K. *Inorg. Chem.* **1996**, *35*, 6809–6815.
(74) Wei, N.; Murthy, N. N.; Karlin, K. D. *Inorg. Chem.* **1994**, *33*, 6093–6100.

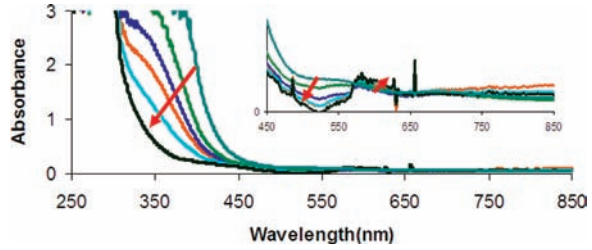

Figure 3. UV−vis spectra at −80 °C in THF, illustrating formation of the $[(CTV\text{-}TMPA)Cu^{II}_3](B(C_6F_5)_4)_3$ upon addition of $[Fe^{III}Cp_2]^+$ (up to 3 equiv, 0.5 equiv each time) to tricopper(I) complex **1**. The downward arrow indicates the changes occurring during the transformation of copper(I) to copper(II). The upward arrow in the inset indicates increase in d-d absorption during addition of $[Fe^{III}Cp_2]^+$, thus formation of copper(II), (λ_{max} = 590 nm). No further spectral changes are observed after addition of 3 equiv $[Fe^{III}Cp_2]^+$.

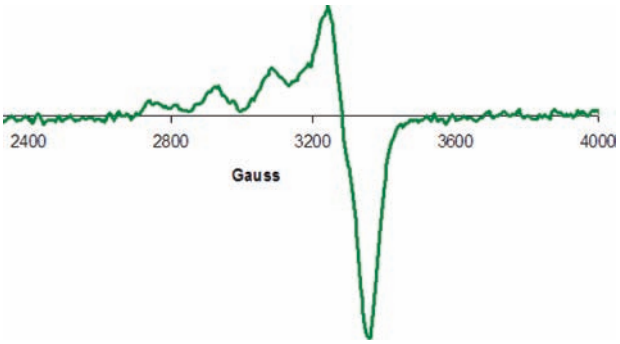

Figure 4. EPR spectrum following reaction of 3 $[Fe^{III}Cp_2]^+$ with $[(CTV\text{-}TMPA)Cu^{I}_3]^{3+}$ (**1**) at 77 K in 2-methyltetrahydrofuran (MeTHF) solvent {EPR parameters, $g_{\|}$ = 2.25, $g_{\perp}$ = 2.05, $A_{\|}$ = 152 G, $A_{\perp}$ = 30 G.}.

$[(CTV\text{-}TMPA)Cu^{II}_3]^{3+}$ (**1-Ox**) (Figure 4), closely correlated in intensity (i.e., semiquantitative spin integration) with EPR spectra of 1.5 equiv of *dimeric* copper(II) complex $[\{(\mathbf{L^{CH_2OMe}})Cu^{II}(Cl)\}_2]^{2+}$ (i.e., 3 equiv of Cu(II)), which in solution breaks up into monomeric species. Thus, we can conclude that all three copper(II) centers are located in a similar tetra-coordinate environment originating from the three equiv of copper centers in this CTV-TMPA ligand system. Species **1-Ox** is insensitive to the presence of O_2.

Generation of $[(CTV\text{-}TMPA)Cu^{I}_3(PPh_3)_3]^{3+}$ (1-PPh$_3$). Triphenylphosphine is well-known as a very good ligand for Cu(I) complexes, and it is sometimes used in the establishing the nature of Cu_nO_2 reactivity or other metal-dioxygen complexes.[9,63,75] The affinity of PPh_3 for copper(I) originates from the soft nature of both species; once a copper(I)-PPh_3 adduct is formed, it is usually unreactive toward O_2.[9,63,75]

The triphenylphosphine adduct of **1**, $[(CTV\text{-}TMPA)Cu^{I}_3(PPh_3)_3]^{3+}$ (**1-PPh$_3$**) may be generated by addition of 3 equiv of PPh_3 to the copper(I) solution of THF and can be isolated by addition of pentane. This product, **1-PPh$_3$**, is stable and insensitive to O_2. We have taken advantage of ^{31}P NMR spectroscopy (with $PMes_3$ internal standard added) to confirm the number of PPh_3 equivalents binding to **1** (Scheme 4). A 1:3 mixture of **1-PPh$_3$** and $P(Mes)_3$ shows that the NMR integration ratios

Scheme 4

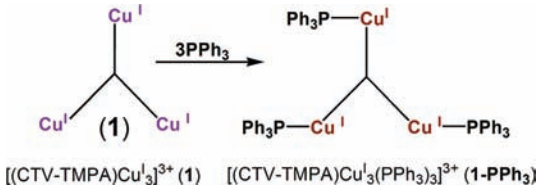

Scheme 5

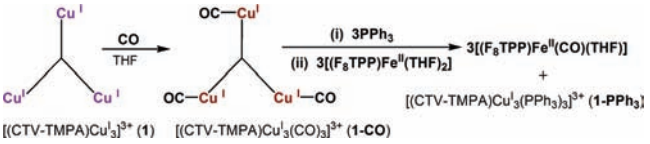

are 1:1.031 for the two peaks observed at 3.79 (**1-PPh$_3$**) and −35.92 ($PMes_3$) ppm, thus indicating three PPh_3 binding sites in $[(CTV\text{-}TMPA)Cu^{I}_3]^{3+}$ (**1**) (Supporting Information, Figure S1),[76] as expected.

Generation of $[(CTV\text{-}TMPA)Cu^{I}_3(CO)_3]^{3+}$ (1-CO) and CO Release by Addition of PPh$_3$. The carbon monoxide adduct of **1**, $[(CTV\text{-}TMPA)Cu^{I}_3(CO)_3]^{3+}$ (**1-CO**) can be generated by bubbling CO through the copper(I) solution (Scheme 5), and the product obtained was characterized by elemental analysis, ^1H NMR and IR spectroscopies. Addition of PPh_3 and quantitative detection of the carbon monoxide released allowed us to confirm that **1-CO** possesses three CO molecules, one per copper. Thus, the amount of CO released from the THF solution of $[(CTV\text{-}TMPA)Cu^{I}_3(CO)_3]^{3+}$ (**1-CO**) upon PPh_3 addition was determined following the addition of 3 equiv of the iron-porphyrinate complex $[(F_8TPP)Fe^{II}(THF)_2]$ {F_8TPP = tetrakis(2,6-difluorophenyl)porphirinate(2-)} {UV−vis (THF; λ_{max}, nm): 421 nm, 542 nm}.[77] The resultant carbonmonoxy-THF complex $[(F_8TPP)Fe^{II}(CO)(THF)]$ {UV−vis (THF; λ_{max}, nm): 411 nm, 525 nm} (also compared with same concentration of $[(F_8TPP)Fe^{II}(THF)_2]$ bubbled with CO) indicated the release of ~2.9 equiv of CO for 1 equiv of $[(CTV\text{-}TMPA)Cu^{I}_3(CO)_3]^{3+}$ (**1-CO**) (Figure 5). Thus, **1-CO** possesses three CO-bound cuprous centers. Consistent with the results described above (i.e., for electrochemistry and the properties of copper in **1-PPh$_3$** and **1-Ox**) the CO bound centers in **1-CO** are comparable since a single IR stretch ($\nu_{C=O}$ = 2094 cm^{-1}) is observed.[76] The ν_{CO} value is typical for that observed for other TMPA analogues (ν_{CO} = 2091−2094 cm^{-1}) and the closest mimic $\mathbf{L^{CH_2OMe}}$ (ν_{CO} = 2094 cm^{-1}).[52,78] This and previous studies indicate an overall tetra-coordinated $Cu^{I}N_3(CO)$ structure (at least as a solid) with one pyridyl group (likely the 6-substituted pyridyl arm) dangling. When all pyridyl groups bond, giving a $Cu^{I}N_4(CO)$ coordination, the ν_{CO} drops to the 2075 cm^{-1} range because of increased Cu^{I}-to-CO back-donation.[78,79]

(75) Paul, P. P.; Tyeklár, Z.; Jacobson, R. R.; Karlin, K. D. *J. Am. Chem. Soc.* **1991**, *113*, 5322–5332.

(76) See the Supporting Information.

(77) Thompson, D. W.; Kretzer, R. M.; Lebeau, E. L.; Scaltrito, D. V.; Ghiladi, R. A.; Lam, K.-C.; Rheingold, A. L.; Karlin, K. D.; Meyer, G. J. *Inorg. Chem.* **2003**, *42*, 5211–5218.

(78) Fry, H. C.; Lucas, H. R.; Narducci Sarjeant, A. A.; Karlin, K. D.; Meyer, G. J. *Inorg. Chem.* **2008**, *47*, 241–256.

(79) Kretzer, R. M.; Ghiladi, R. A.; Lebeau, E. L.; Liang, H.-C.; Karlin, K. D. *Inorg. Chem.* **2003**, *42*, 3016–3025.

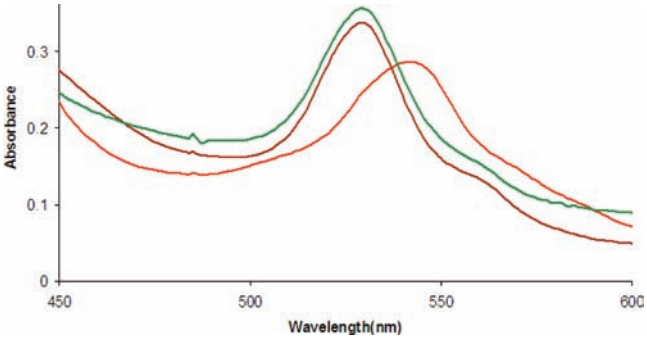

Figure 5. UV−vis absorption spectra of $[(F_8TPP)Fe^{II}(THF)_2]$ in THF (red) at −90 °C and the spectra generated after addition of CO to generate $[(F_8TPP)Fe^{II}(CO)(THF)]$ (brown). The green spectrum is generated from a separate (same final copper concentration as that for red spectrum) addition of $[(F_8TPP)Fe^{II}(THF)_2]$ to the solution of $3PPh_3$ plus $[(CTV\text{-}TMPA)Cu^{I}_3(CO)_3]^{3+}$ (**1-CO**). A ∼2.9 equiv $[(F_8TPP)Fe^{II}(CO)(THF)]$ formation is indicated (after baseline correction).

Generation of $[(CTV\text{-}TMPA)Cu^{II}_3(Cl)_3](B(C_6F_5)_4)_3$ (1-Cl) via a Dechlorination Reaction. As we have seen many times previously and is known in other cases, TMPA-based copper(I) complexes are reactive toward organohalides, resulting in the production of halide-copper(II) products.[52,72] A recent report from our laboratories suggests such reactions may occur via organocopper intermediates.[80] Here, we utilized this organohalide reaction chemistry (eq 1) to generate a chloride complex $[(CTV\text{-}TMPA)Cu^{II}_3(Cl)_3](B(C_6F_5)_4)_3$ (**1-Cl**). Exposure of **1** to $CHCl_3$ (in THF) at RT led to an immediate reaction (according to eq 1), and **1-Cl** was isolated in high yield.

$$[(CTV\text{-}TMPA)Cu_3{}^{I}]^{3+} + 3R\text{-}X \rightarrow [(CTV\text{-}TMPA)Cu^{II}(X)_3]^{3+} + \text{unknown products} \quad (1)$$

EPR spectroscopy (Supporting Information, Figure S3), elemental analysis, cyclic voltammetry (Supporting Information, Figure S4), and ESI-MS (Supporting Information, Figures S10 and S11) studies of **1-Cl** were carried out.[76] An ESI-MS spectrum of $[(CTV\text{-}TMPA)Cu^{II}_3(Cl)_3](ClO_4)_3$ (in CH_3CN at RT) showed strong peaks in the range m/z = 1808−1814 for $(CTV\text{-}TMPA)Cu^{II}_3(Cl)_3(ClO_4)_2{}^{+}$, and the observed peak pattern matched well with that predicted.[76] The bromide analogue $[(CTV\text{-}TMPA)Cu^{II}_3(Br)_3]^{3+}$ was also synthesized following a similar method involving dehalogenation of $CHBr_3$ with $[(CTV\text{-}TMPA)Cu^{I}_3]^{3+}$; the EPR (Supporting Information, Figure S8) and ESI-MS (Supporting Information, Figures S12 and S13) spectra was recorded. ESI-MS spectra of $[(CTV\text{-}TMPA)Cu^{II}_3(Br)_3](ClO_4)_3$ (in CH_3CN at RT) showed strong peaks at m/z = 1940−1948 for $(CTV\text{-}TMPA)Cu^{II}_3(Br)_3(ClO_4)_2{}^{+}$, and the observed peak pattern matched well with that theoretically predicted.[76] The synthesis of $[(L^{CH_2OMe})Cu^{II}(Cl)]B(C_6F_5)_4$ was previously reported. As related to present study, EPR and cyclic voltammetry studies of $[(L^{CH_2OMe})Cu^{II}(Cl)]B(C_6F_5)_4$ were carried out, and

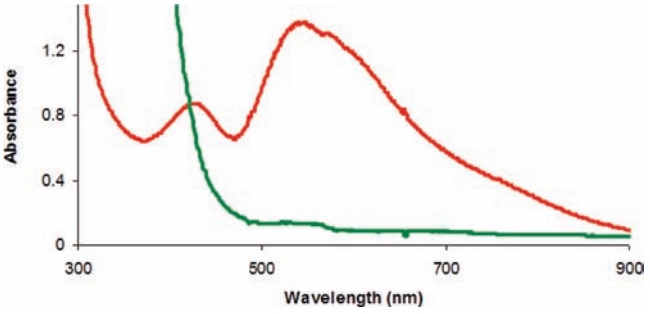

Figure 6. UV−vis spectra at −80 °C in THF, illustrating formation of **1-O₂** (red) from $[(CTV\text{-}TMPA)Cu^{I}_3]^{3+}$ (**1**) (green) plus dioxygen. See text for assignments of the 427 and 543 nm absorptions.

the peak pattern and positions were found to be very similar to that for $[(CTV\text{-}TMPA)Cu^{II}_3(Cl)_3]^{3+}$ (**1-Cl**).

Reaction of O_2 with $[(CTV\text{-}TMPA)Cu^{I}_3]^{3+}$ (1). The copper chemistry of the mononuclear mimic (L^{CH_2OMe}) of the copper sites in CTV-TMPA has been recently reported. Copper(I)/O_2 reactivity of L^{CH_2OMe} leads to formation of a dinuclear purple species (similar to parent TMPA) formulated as $[\{(L^{CH_2OMe})Cu^{II}\}_2(\mu\text{-}1,2\text{-}O_2{}^{2-})]^{2+}$ (**2-O₂**; see diagram below) based on its UV−vis {λ_{max} = 540 nm (ε, 9550 M^{-1} cm^{-1}) and 610 nm, sh, (ε, 6500 M^{-1} cm^{-1})} and rR ($\nu_{(O-O)}$ = 848 ($\Delta[^{18}O_2]$ = −47) cm^{-1}, $\nu_{(Cu-O)}$ = 550 ($\Delta[^{18}O_2]$ = −26 cm^{-1} in THF) spectroscopic properties.[81] We have also recently characterized the first formed mononuclear Cu^{I}/O_2 initial adduct with a TMPA derivative, NMe_2-TMPA {tris(2-(4-dimethylaminopyridyl)methyl)amine}, leading to a brilliant green colored copper-superoxo species $[(NMe_2\text{-}TMPA)Cu^{II}(O_2{}^{-})]^{+}$ (see diagram below): λ_{max} = 418 (ε = 4300 M^{-1} cm^{-1}), 615 (ε = 1100 M^{-1} cm^{-1}), and 767 (ε = 840 M^{-1} cm^{-1}) and rR spectroscopy ($\nu_{(O-O)}$ = 1121 ($\Delta[^{18}O_2]$ = −63) cm^{-1}, $\nu_{(Cu-O)}$ = 472 ($\Delta[^{18}O_2]$ = −20 cm^{-1} in THF).[82]

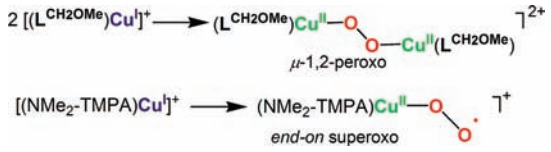

Following oxygenation of $[(CTV\text{-}TMPA)Cu^{I}_3]^{3+}$ (**1**) in THF at −80 °C, there was a rapid change from colorless to an intense purple colored solution. The UV−vis spectrum of this product **1-O₂** (Figure 6) includes intense features at 543 and 427 nm. The former absorption, along with lower broad energy closely resembles the distinctive pattern known for the "parent" complexes $[\{(TMPA)Cu^{II}\}_2(\mu\text{-}1,2\text{-}O_2{}^{2-})]^{2+}$ (**3-O₂**) and $[\{(L^{CH_2OMe})Cu^{II}\}_2(\mu\text{-}1,2\text{-}O_2{}^{2-})]^{2+}$ (**2-O₂**), as well as other structurally similar *trans*-peroxo binuclear Cu_2O_2-adducts.[5,81] This is confirmed by rR spectroscopy, vide infra.

rR Spectroscopy of Solutions from $[(CTV\text{-}TMPA)Cu^{I}_3]^{3+}$ (1)/O_2. rR spectra of **1-O₂** were collected

(80) Maiti, D.; Narducci Sarjeant, A. A.; Itoh, S.; Karlin, K. D. *J. Am. Chem. Soc.* **2008**, *130*, 5644–5645.

(81) Maiti, D.; Woertink, J. S.; Narducci Sarjeant, A. A.; Solomon, E. I.; Karlin, K. D. *Inorg. Chem.* **2008**, *47*, 3787–3800.

(82) Maiti, D.; Fry, H. C.; Woertink, J. S.; Vance, M. A.; Solomon, E. I.; Karlin, K. D. *J. Am. Chem. Soc.* **2007**, *129*, 264–265.

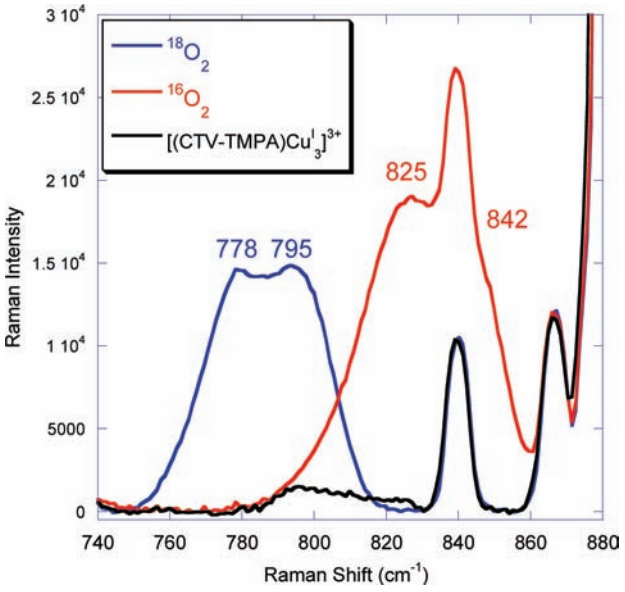

Figure 7. rR spectra (ν_{O-O} region) of $[(CTV\text{-}TMPA)Cu^{I}_3]^{3+}$ (**1**) (black), **1**-^{16}**O$_2$** (red), and **1**-^{18}**O$_2$** (blue) (λ_{excit} = 530 nm at 77 K) in THF (1.0 mM **1**).

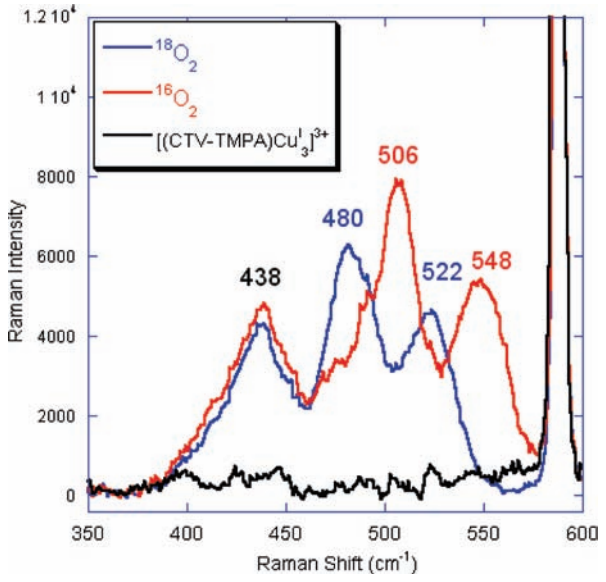

Figure 8. rR spectra (ν_{Cu-O} region) of $[(CTV\text{-}TMPA)Cu^{I}_3]^{3+}$ (**1**) (black), **1**-^{16}**O$_2$** (red), and **1**-^{18}**O$_2$** (blue) (λ_{excit} = 530 nm at 77 K) in THF (1.0 mM **1**).

with λ_{excit} = 530 nm with $^{16}O_2$ and $^{18}O_2$ isotopic substitution. For **1-O$_2$** sample concentrations of ~1.0 mM in THF, two isotope-dependent stretches were observed at 842 and 825 cm^{-1}, which shift to 795 and 778 cm^{-1} upon $^{18}O_2$ substitution and are assigned as peroxo O−O stretches (Figure 7). In addition, there are two isotope-sensitive stretches observed at 506 and 548 cm^{-1}, which shift to 480 and 522 cm^{-1} and are assigned as symmetric Cu−O stretches (Figure 8). An $^{18}O_2$-insensitive stretch is observed at 438 cm^{-1} and is assigned as a Cu−N_{amine} stretch. Cu−N_{py} ligand vibrations could be resolved in some cases (vide infra), but here for complex **1-O$_2$**, an overlapping solvent band from THF (258 cm^{-1}), precludes its observation.

The frequencies and 18-O shifts observed for **1-O$_2$** correlate well to those of an μ-1,2-end-on peroxo species, Table 2.[5] For $[(CTV\text{-}TMPA)Cu^{I}_3]^{3+}$ (**1**)/O_2 derived solutions, both UV−vis absorption and rR data in the peroxo region (with λ_{excit} = 530 nm) are very similar to those observed for the parent $[\{(\mathbf{L}^{\mathbf{CH_2OMe}})Cu^{II}(\mu\text{-}1,2\text{-}O_2^{2-})\}_2]^{2+}$ (**2-O$_2$**) complex. As was previously observed for the parent $\mathbf{L}^{\mathbf{CH_2OMe}}$ complex, shifts in the rR and absorption peak positions relative to $[\{(TMPA)Cu^{II}(\mu\text{-}1,2\text{-}O_2^{2-})\}_2]^{2+}$ (**3-O$_2$**) arise from the presence of 6-substituted pyridyl arms of the TMPA.[81]

The UV−vis spectra of solutions generated from O_2 reaction with $[(CTV\text{-}TMPA)Cu^{I}_3]^{3+}$ (**1**) also show a prominent absorption feature at 427 nm (Figure 6). rR spectra were collected with λ_{excit} = 413 nm, and an O−O stretch at 1129 cm^{-1}, shifting to 1069 cm^{-1} upon $^{18}O_2$ substitution, was observed (Figure 9). This stretching frequency and isotopic shift, along with the position and intensity of the 427 nm absorption, are consistent with those of a mononuclear superoxo-copper(II) complex.[5,82,83] A Cu−O stretch was also observed for the complex with 413 nm excitation at 463 cm^{-1}, shifting to 436 cm^{-1} upon $^{18}O_2$ substitution (Figure 10).

Interestingly, rR spectra collected with λ_{excit} = 530 nm on samples at higher concentration (1.53 mM of **1**) show only one O−O stretch at 825 cm^{-1} ($\Delta(^{18}O_2)$ = −47; Figure 11) and a Cu−O stretching at 506 cm^{-1} ($\Delta(^{18}O_2)$ = −26; Figure 12).[84] Thus, at this higher concentration, only one peroxo species is observed. This result confirms that for the 1.0 mM sample concentration, the 506 cm^{-1} symmetric Cu−O and the 825 cm^{-1} O−O stretches derive from one peroxo complex, while the 548 cm^{-1} symmetric Cu−O and 842 cm^{-1} O−O stretches derive from a second, distinct peroxo complex.

The UV−vis and rR spectroscopic data indicate that both the superoxo and the peroxo species form from $[(CTV\text{-}TMPA)Cu^{I}_3]^{3+}$ (**1**)/O_2 chemistry. In THF at 1.0 mM concentration, one type of superoxo (O_2^-) and two different types of peroxo (μ-1,2-O_2^{2-}) species are present (Figure 7 and 8). Thus, a total of three different species are formed from **1**/O_2. Interestingly, oxygenation with a more concentrated copper solution (1.53 mM of **1**) in THF results in only one of the peroxo species and the superoxo species, as evidenced by rR spectroscopy (vide supra). The two different μ-1,2-peroxos observed at a lower concentration are likely an intra- and intermolecular species, while at higher concentration the observed peroxo is likely an *inter*molecular species. This type of

(83) Itoh, S. *Curr. Opin. Chem. Biol.* **2006**, *10*, 115–122.

(84) The unequal intensities of the two Cu−O stretches shown in Figure 12 is the result of two factors. First, this intensity difference (also reflected in the intensity differences in the ν(O−O)'s in Figure 11) reflects minor differences in the concentration of $^{16}O_2$ vs $^{18}O_2$ **1-O$_2$** samples. The concentration of **1-O$_2$** is slightly lower for the $^{18}O_2$-generated sample presented than for the $^{16}O_2$-generated sample. The second factor, which introduces error in intensity ratios (particularly for spectra with lower signal-to-noise ratio as for Figures 11 and 12) is the method used to scale the spectra. Each spectrum presented is scaled to a nearby THF solvent mode, which is used as an internal standard. The spectrum shown in Figure 12 was scaled to the weak 586 cm^{-1} THF vibration while the O−O stretches shown in Figure 11 were scaled to the intense 880 cm^{-1} THF vibration. Thus error is introduced into the peak intensities as a result of the scaling procedure used in processing the rR data. The error in the calculated intensity of the weak 586 cm^{-1} THF vibration results in error in the final intensity of the scaled Cu−O stretches in Figure 12.

Table 2. Spectroscopic Features for Copper-Dioxygen Adducts Related to Those Observed in **1**/O_2 Solutions

	solvent	UV−vis/nm (ε∼M^{-1} cm^{-1})	ν, cm^{-1}, $^{16}O-^{16}O$ ($^{18}O-^{18}O$)	ν, cm^{-1}, Cu−^{16}O (Cu−^{18}O)	ref
		μ-1,2-Peroxodicopper(II)-Complexes			
$[(CTV\text{-}TMPA)Cu^{II}_m(\mu\text{-}1,2\text{-}O_2^{2-})]^{n+}$ (**1-O$_2$**) (1.0 mM)	THF	543 (9650), 605 (8100)	842 (795) 825 (778)	506 (480) 548 (522)	a
$[(CTV\text{-}TMPA)Cu^{II}_m(\mu\text{-}1,2\text{-}O_2^{2-})]^{n+}$ (**1-O$_2$**) (1.53 mM)	THF		825 (778)	506 (480)	a
$[\{(TMPA)Cu^{II}\}_2(\mu\text{-}1,2\text{-}O_2^{2-})]^{2+}$ (**3-O$_2$**) (parent complex)	EtCN	525 (11300), 615 (5800)	832 (788)	561 (535)	86
	Et_2O	520 (19200)	827 (783)	561 (535)	87
$[\{(L^{CH_2OMe})Cu^{II}\}_2(\mu\text{-}1,2\text{-}O_2^{2-})]^{2+}$ (**2-O$_2$**)	THF	540 (9550), 610 (6500)	848(801)	550(524)	81
		End-on Bound $Cu^{II}(O_2^{\bullet-})$ Complex			
$[(CTV\text{-}TMPA)Cu^{II}_x(O_2^{\bullet-})]^{y+}$ (**1-O$_2$**) (1.0 mM)	THF	427 (3150)	1129 (1069)	463 (436)	a
$[(Me_2N\text{-}TMPA)Cu^{II}(O_2^{\bullet-})]^{+}$	THF	418 (4300)	1121 (1058)	472 (452)	82
$[(TMG_3tren)Cu^{II}(O_2^{\bullet-})]^{+}$	Acetone	447 (3400)	1117 (1059)	b	88

[a] This work. [b] Not reported.

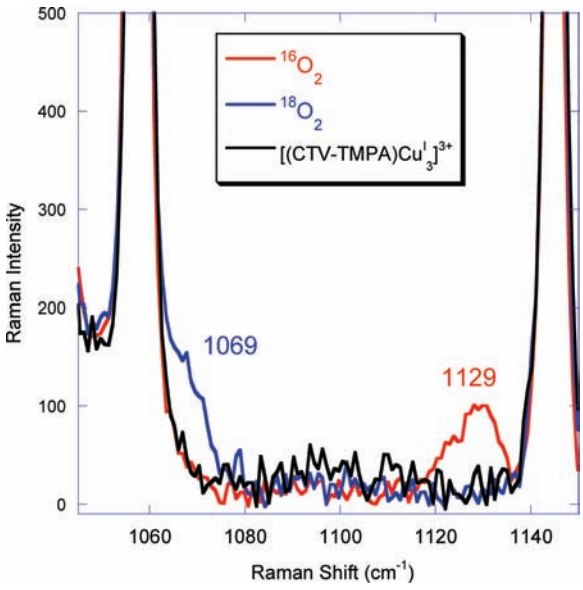

Figure 9. rR spectra (ν_{O-O} region) of $[(CTV\text{-}TMPA)Cu^{I}_3]^{3+}$(**1**) (black), **1-$^{16}O_2$** (red), and **1-$^{18}O_2$** (blue) ($\lambda_{excit}$ = 413 nm at 77 K) in THF (1.0 mM **1**).

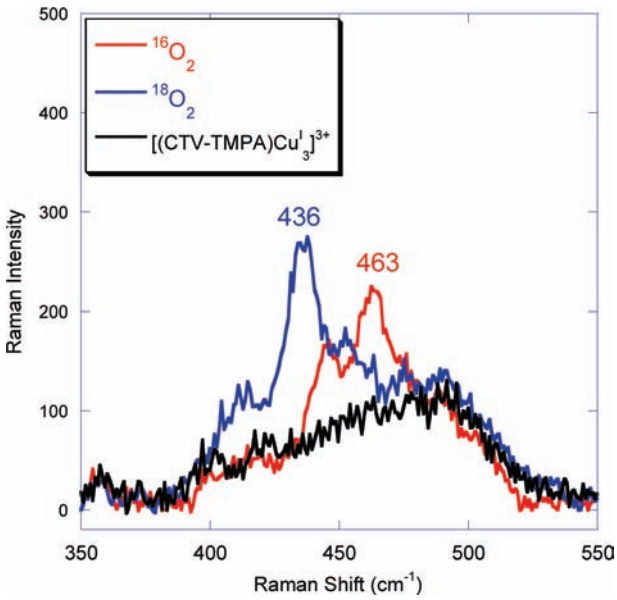

Figure 10. rR spectra (ν_{Cu-O} region) of $[(CTV\text{-}TMPA)Cu^{I}_3]^{3+}$(**1**) (black), **1-$^{16}O_2$** (red), and **1-$^{18}O_2$** (blue) ($\lambda_{excit}$ = 413 nm at 77 K) in THF (1.0 mM **1**).

concentration dependent behavior has been previously observed.[85] Thus, to our knowledge, oxygenation of tricopper(I) complex **1** leads to the first example of synthetic copper complex which can simultaneously stabilize a mononuclear superoxo and dinuclear peroxo species (vide infra).

Decomposition of $[(CTV\text{-}TMPA)Cu^{I}_3]^{3+}$(1)/$O_2$ Derived Adducts. Previous systematic studies with tetradentate ligand-copper(I)/O_2 systems show that the superoxo and peroxo species are both favored enthalpically but strongly disfavored entropically, accounting for their instability at higher temperatures.[53] As shown (vide supra), oxygenation of **1** results in a mixture of binuclear peroxo (one or two species) and mononuclear superoxo complexes. While UV−vis and rR spectra could be obtained, in fact these species are moderately unstable and complete decomposition occurs within ∼2 h even at −80 °C (Figure 13). We also note that both superoxo and peroxo species appear to decompose at the same rate, and a purple (λ_{max} = 685 nm) colored solid could be obtained by workup at RT. Although it appeared as a homogeneous material, the exact nature of this species could not be determined (but see the Experimental Section).

$[(CTV\text{-}TMPA)Cu^{I}_3]^{3+}$(1) Reaction with Sulfur. Recently we described the reversible reaction of $[(L^{CH_2OMe})Cu^{I}]^{+}$ (**2**) with elemental sulfur, the result being the formation of a single complex, the end-on bound disulfide-dicopper(II) complex $[\{(L^{CH_2OMe})\text{-}Cu^{II}\}_2(\mu\text{-}1,2\text{-}S_2^{2-})]^{2+}$ (**2-S**) {λ_{max} = 540 nm, $\nu_{(S-S)}$ = 492 cm^{-1}; $\nu_{(Cu-S)sym}$ = 309 cm^{-1}} (Table 3).[52] This contrasts somewhat with the behavior of the parent complex where $[(TMPA)Cu^{I}(CH_3CN)]^{+}$(**3**)/$S_8$ chemistry produces an equilibrium mixture of at least three complexes. Yet, an X-ray structure obtained corresponds

(85) Pidcock, E.; Obias, H. V.; Abe, M.; Liang, H.-C.; Karlin, K. D.; Solomon, E. I. *J. Am. Chem. Soc.* **1999**, *121*, 1299–1308.
(86) Baldwin, M. J.; Ross, P. K.; Pate, J. E.; Tyeklár, Z.; Karlin, K. D.; Solomon, E. I. *J. Am. Chem. Soc.* **1991**, *113*, 8671–8679.
(87) Jacobson, R. R.; Tyeklár, Z.; Karlin, K. D.; Liu, S.; Zubieta, J. *J. Am. Chem. Soc.* **1988**, *110*, 3690–3692.
(88) Schatz, M.; Raab, V.; Foxon, S. P.; Brehm, G.; Schneider, S.; Reiher, M.; Holthausen, M. C.; Sundermeyer, J.; Schindler, S. *Angew. Chem., Int. Ed.* **2004**, *43*, 4360–4363.

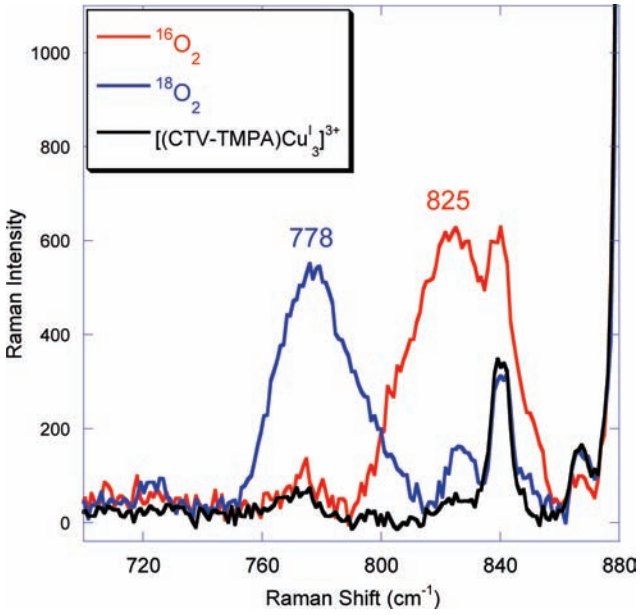

Figure 11. rR spectra (ν_{O-O} region) of $[(CTV\text{-}TMPA)Cu^{I}_3]^{3+}$ (**1**) (black), **1-$^{16}O_2$** (red), and **1-$^{18}O_2$** (blue) (at 77 K, λ_{excit} = 530 nm) in THF (1.53 mM **1**).

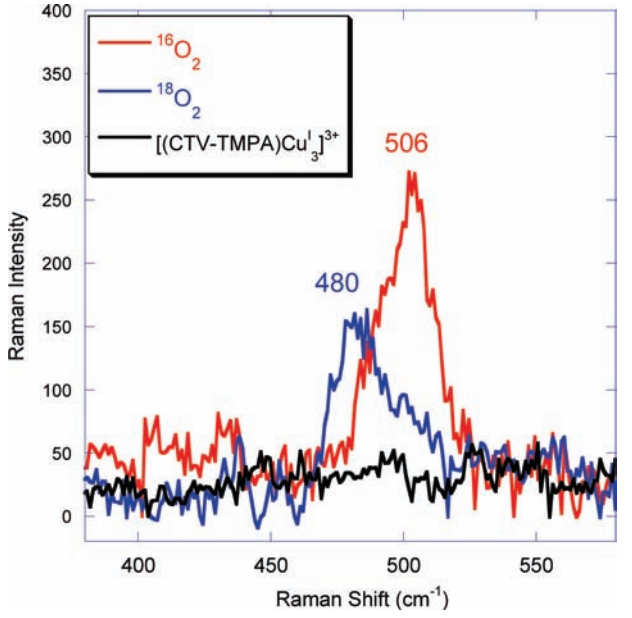

Figure 12. rR spectra (ν_{Cu-O} region) of $[(CTV\text{-}TMPA)Cu^{I}_3]^{3+}$ (**1**) (black), **1-$^{16}O_2$** (red), and **1-$^{18}O_2$** (blue) (at 77 K, λ_{excit} = 530 nm) in THF (1.53 mM **1**).

to $[\{(TMPA)Cu^{II}\}_2(\mu\text{-}1,2\text{-}S_2^{2-})]^{2+}$ (**3-S**); rR spectroscopic for **3-S** could also be elucidated.[89,90] As noted, the only difference between TMPA and $\mathbf{L^{CH_2OMe}}$ is the presence of the pyridyl 6−CH_2−O−R motif in the latter, and of course this is present for all three copper ion binding cites within CTV-TMPA. Thus, we expected that $[(CTV\text{-}TMPA)Cu^{I}_3]^{3+}$ (**1**)/S_8 chemistry might also generate characterizable end-on

(89) Chen, P.; Fujisawa, K.; Helton, M. E.; Karlin, K. D.; Solomon, E. I. *J. Am. Chem. Soc.* **2003**, *125*, 6394–6408.

(90) Helton, M. E.; Chen, P.; Paul, P. P.; Tyeklár, Z.; Sommer, R. D.; Zhakarov, L. N.; Rheingold, A. L.; Solomon, E. I.; Karlin, K. D. *J. Am. Chem. Soc.* **2003**, *125*, 1160–1161.

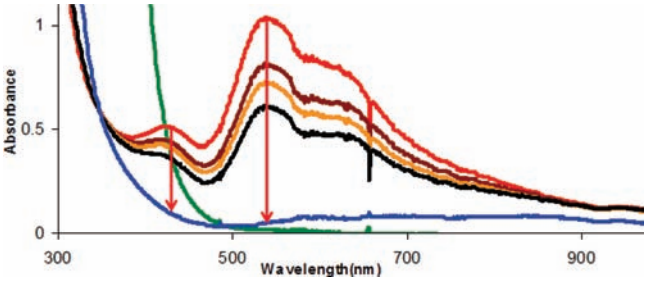

Figure 13. UV−vis spectra at −80 °C in THF, illustrating the decomposition (i.e., thermal transformation) of purple Cu−O_2 species (**1-O_2**). $[(CTV\text{-}TMPA)Cu^{I}_3]^{3+}$ (**1**) (green spectrum) following bubbling with O_2 generates **1-O_2** (red spectrum) which then undergoes subsequent transformations (brown, orange, and black spectra) leading finally to a final **1-Dec** species (blue spectrum). Also, see Experimental Section.

bound disulfide-dicopper(II) complexes similar to what occurs for **2-S** (Table 3).

Addition of elemental sulfur (as S_8)[91] to **1** at −80 °C under argon causes an immediate change in color of the solution from yellow to purple; such solutions are very stable, but decreased absorptions occur rapidly even upon slight warming. As described above, $[(CTV\text{-}TMPA)Cu^{I}_3]^{3+}$ (**1**) reacts rapidly and irreversibly with O_2 at RT; however, it is required that lower temperatures be used to characterize and study Cu^{I}_3/O_2 adducts.[5] Titrations of S_8 with $[(CTV\text{-}TMPA)Cu^{I}_3]^{3+}$ (**1**) show that (based on UV−vis criteria, and rR spectroscopy, see below, Table 3) only one species forms in solution, $[\{(CTV\text{-}TMPA)Cu^{II}_3\}_2(\mu\text{-}1,2\text{-}S_2^{2-})_3]^{6+}$ (**1-S**), λ_{max} = 544 nm (Figure 14). The proposed structure for **1-S** is shown in the diagram here and discussed further below.

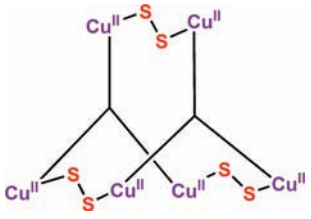

Temperature Dependent Sulfur Binding in $[(CTV\text{-}TMPA)Cu^{I}_3]^{3+}$ (1). We find that by varying the temperature of solutions of $[(CTV\text{-}TMPA)Cu^{I}_3]^{3+}$(**1**)/$S_8$, we can nicely vary the extent of sulfur binding. Heating/cooling cycles on solutions of $[(CTV\text{-}TMPA)Cu^{I}_3]^{3+}$(**1**)/$S_8$ could be easily carried out (Figure 15). That elemental sulfur is released from a warmed (to RT) −80 °C solution is evident from the fact that no sulfur from an outside source is needed to fully reform the purple solution upon recooling. The cycle can be repeated multiple times without addition of more S_8 or an absorbance intensity change. We note that the dioxygen reactivity of $[(CTV\text{-}TMPA)Cu^{I}_3]^{3+}$ (**1**) is not similarly reversible. We also note that a similar temperature variation of $[\{(\mathbf{L^{CH_2OMe}})\text{-}Cu^{II}\}_2(\mu\text{-}1,2\text{-}S_2^{2-})]^{2+}$ (**2-S**) resulted in complete loss of

(91) Elemental sulfur can exist in solution in a number of forms other than S_8, see page 499 in: Cotton, F. A.; Wilkinson, G., *Advanced Inorganic Chemistry*, 6th ed.; John Wiley: New York. Here, we will consistently describe the chemistry and reaction chemistry in terms of use of S_8.

Table 3. Summary of Spectroscopic Features for Related Copper−Sulfur Adducts

μ-1,2-disulfide-dicopper(II) -complexes	solvent	UV−vis/nm ($\varepsilon\sim M^{-1}$ cm^{-1})	ν, cm^{-1}, ^{32}S−^{32}S (^{34}S−^{34}S)	ν, cm^{-1}, Cu−^{32}S (Cu−^{34}S)	ref
[{(CTV-TMPA)Cu^{II}_3}$_2$(μ-1,2-S_2^{2-})$_3$]$^{6+}$ (**1-S**)	THF	544 (7270)	489(479)	307(302)	a
[{(TMPA)Cu^{II}}$_2$(μ-1,2-S_2^{2-})]$^{2+}$ (**3-S**)	CH_3CN	568[b]	499(490)	316(312)	90
[{(L^{CH_2OMe})Cu^{II}}$_2$(μ-1,2-S_2^{2-})]$^{2+}$ (**2-S**)	THF	540(4600)[c]	492(482)	309(304)	52

[a] This work. [b] THF. [c] 2-methyltetrahydrofuran.

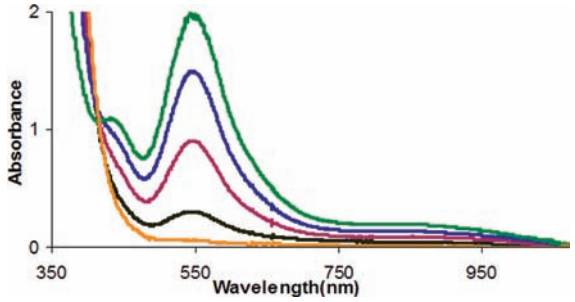

Figure 14. UV−vis spectra at −80 °C in tetrahydrofuran (THF) solvent, illustrating that only the end-on disulfide complex [{(CTV-TMPA)Cu^{II}_3}$_2$(μ-1,2-S_2^{2-})$_3$]$^{6+}$ (**1-S**) is generated from [(CTV-TMPA)Cu^{I}_3]$^{3+}$(**1**)/4S. The yellow/orange spectrum is that for [(CTV-TMPA)Cu^{I}_3]$^{3+}$(**1**); addition of increasing amounts of sulfur results leads to the spectra shown in black (1S), brownish-purple (2S), blue (3S), and green (4S). No spectral changes were observed upon further addition of sulfur to the reaction solution.

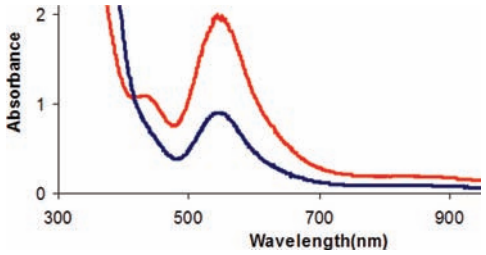

Figure 15. UV−vis spectra at −80 °C in THF, illustrating formation of the end-on disulfide complex [{(CTV-TMPA)Cu^{II}_3}$_2$(μ-1,2-S_2^{2-})$_3$]$^{6+}$ (**1-S**) from [(CTV-TMPA)Cu^{I}_3]$^{3+}$(**1**)/S_8 reactivity (red spectrum). The blue spectrum shown resulted upon warming a solution of **1-S** (red spectrum). Recooling to −80 °C again leads to the reformation of the red spectrum. This cycle can be repeated several times (see text).

sulfur at RT.[52] However, in the present case, **1-S** did retain some sulfur coordination even at RT. Thus, attempts to isolate solid **1-S** (with decreased intensity, hence a mixture of **1** and **1-S**) were carried out successfully, and (re)dissolving the solid material showed a similar intensity to that of a warmed-up solution resulting from **1**/sulfur reactivity.

[(CTV-TMPA)Cu^{I}_3]$^{3+}$(1)/S_8 Product rR Spectroscopy. rR spectra of [(CTV-TMPA)Cu^{I}_3]$^{3+}$ (**1**)/S_8 with ^{32}S and ^{34}S isotopic substitution were collected with λ_{ex} = 530 nm at 77 K. The peaks at 494 cm^{-1} and 307 cm^{-1} shift to 482 cm^{-1} and 302 cm^{-1}, respectively, with ^{34}S isotopic substitution (Figure 16). On the basis of spectral similarities with [{(L^{CH_2OMe})Cu^{II}}$_2$(μ-1,2-S_2^{2-})]$^{2+}$ (**2-S**),[93] we can assign the complex as having a single type of end-on μ-1,2 disulfido-dicopper(II) complex, [{(CTV-TMPA)-Cu^{II}_3}$_2$(μ-1,2-S_2^{2-})$_3$]$^{6+}$ (**1-S**). The 307 cm^{-1} peak can be assigned as a ν(Cu−S)$_{sym}$ vibration. The peaks at 494 cm^{-1} and 476 cm^{-1} in the ^{32}S Raman spectrum are the result

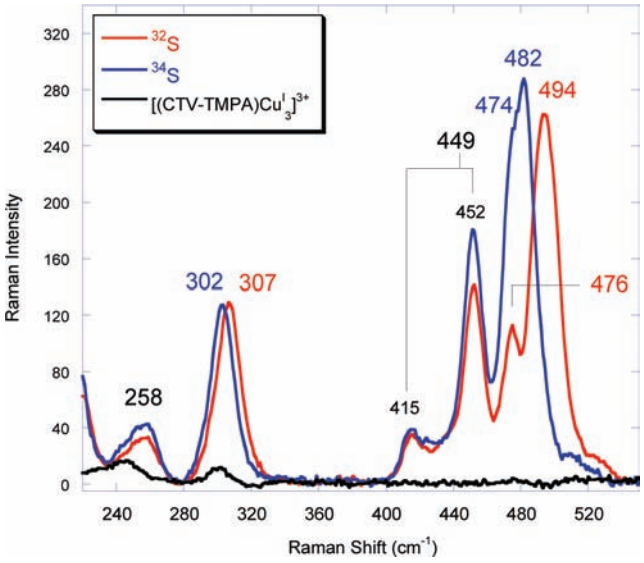

Figure 16. rR spectra of **1-S** with naturally abundant sulfur (red) and with isotopically enriched ^{34}S (blue) in THF (λ_{excit} = 530 nm, 77 K).

of a Fermi resonance of the ν(S−S) peak with a local non-enhanced mode of the same symmetry and correspond to a pre-interaction ν(S−S) of 489 cm^{-1}.[52]

The high ν(S−S) value of 489 cm^{-1} for [{(CTV-TMPA)Cu^{II}_3}$_2$(μ-1,2-S_2^{2-})$_3$]$^{6+}$ (**1-**^{32}**S**), which was also observed previously for [{(TMPA)Cu^{II}}$_2$(μ-1,2-S_2^{2-})]$^{2+}$ (**3-S**) and [{(L^{CH_2OMe})Cu^{II}}$_2$(μ-1,2-S_2^{2-})]$^{2+}$ (**2-S**), is indicative of the strong interaction between the S_2^{2-} and Cu^{II} ion centers, which removes electron density from the S−S π^*_σ orbital and leads to a strengthened S−S bond. The 259 cm^{-1} is assigned as a ν(Cu−N)$_{py}$ stretch,[92] and the two additional Raman peaks, observed at 415 and 452 cm^{-1}, are the result of a Fermi splitting of ν(Cu−N)$_{amine}$ and correspond to a pre-interaction ν(Cu−N)$_{amine}$ of 449 cm^{-1}.

Complex Formulation; Proposed Structure. We suggest that the product of the [(CTV-TMPA)Cu^{I}_3]$^{3+}$(**1**)/S_8 reaction is a hexanuclear complex [{(CTV-TMPA)Cu^{II}_3}$_2$(μ-1,2-S_2^{2-})$_3$]$^{6+}$ (**1-S**) (see diagram above) (λ_{max} = 544 nm, Figure 14). This proposal derives from the very close similarity in characteristic UV−vis and rR spectroscopic features of **1-S** as compared to the well characterized and comparable complexes employing the L^{CH_2OMe} and TMPA ligands. Complex **1-S** possesses only the [{(ligand)Cu^{II}}$_2$(μ-1,2-S_2^{2-})]$^{2+}$ moiety, a binuclear structure. Thus, for our CTV-TMPA tricopper framework, the simplest formulation and complex likely to fulfill this requirement of possessing equivalent binuclear

(92) The high concentration of **1-S** used for the rR data presented in Figure 16 (2.45 mM) resulted in an intense, well-resolved ν(Cu−N)py peak which could be reproducibly observed over the solvent vibrations.

units would be the hexanuclear complex depicted in the diagram above. Determination of the exact structure would have to await an X-ray structure determination.

Summary/Conclusions

Our continuing efforts into modeling the active sites of copper-cluster containing enzymes have led us to synthesize CTV-based trinucleating ligand, CTV-TMPA, which employs tetradentate chelates as their copper binding sites. A series of chemical studies with the copper(I)-complex of CTV-TMPA, $[(\text{CTV-TMPA})\text{Cu}^{\text{I}}_3]^{3+}$, were carried out, including cyclic voltammetry, CO-binding and release, PPh_3-binding, complete oxidation of copper centers to a tricopper-(II) complex, and oxidative dehalogenation chemistry. The Cu^{I}/O_2 chemistry leads to the first example of a synthetic copper complex which can stabilize a mononuclear superoxo and dinuclear peroxo species simultaneously within one system. The rR studies of CTV-TMPA-$\text{Cu}_3^{\text{I}}/O_2$ adduct(s) at lower concentration (1.0 mM) demonstrate two types of end-on peroxo and one type of superoxo species, whereas at a bit higher concentration (1.53 mM), formation of only one type of peroxo along with a superoxo species are observed. The reaction of elemental sulfur with $[(\text{CTV-TMPA})\text{Cu}^{\text{I}}_3]^{3+}$ (**1**) leads to formation of a single dicopper-disulfide moiety with characteristic UV−vis and rR spectroscopic signatures, proposed to lead to an overall hexanuclear structure.

Our newly designed CTV based trinuclear ligand and tricopper(I) chemistry at this point appears not to lead to O_2-chemistry which might bear on, for example, the cooperative tricopper/O_2 reactivity observed in MCOs. Still, we have learned and we think advanced our knowledge and thinking about copper ion cluster design and chemistry.[93] The seemingly daunting task to design tri- or tetranuclear copper complexes which might mediate efficient dioxygen four-electron reduction (of interest in MCO (bio)chemistry or in fuel cell catalysts design) remains of great significance and interest.

Acknowledgment. This work was supported by grants from the National Institutes of Health (K.D.K., GM28962; E.I.S., DK31450).

Supporting Information Available: Additional information as noted in the text. This material is available free of charge via the Internet at http://pubs.acs.org.

(93) Perhaps the 6-CH_2-O linker between the TMPA and CTV units is too flexible, and a more rigid connection via synthetically constraining of the three chelates moieties would facilitate tricopper/small molecule interactions.